JVI Accepted Manuscript Posted Online 27 September 2017 J. Virol. doi:10.1128/JVI.01455-17 Copyright © 2017 American Society for Microbiology. All Rights Reserved.

1 Genome-wide mutagenesis of dengue virus reveals plasticity of the NS1

2 protein and enables generation of infectious tagged reporter viruses

- 3
- 4 Nicholas S. Eyre ^{a,b,*,1}, Stephen M. Johnson ^{a,b,1,2}, Auda A. Eltahla ^c, Maria Aloi ^{a,b,3}, Amanda
- 5 L. Aloia^d, Christopher A. McDevitt^a, Rowena A. Bull^c, Michael R. Beard^{a,b,*}
- 6
- ^a Research Centre for Infectious Diseases, School of Biological Sciences, University of
- 8 Adelaide, Adelaide, Australia
- 9 ^b Centre for Cancer Biology, SA Pathology, Adelaide, Australia
- ^c Viral Immunology Systems Program (VISP), School of Medical Sciences, The Kirby
- 11 Institute, UNSW, Sydney, Australia
- ¹² ^d Cell Screen SA, Flinders Centre for Innovation in Cancer, Flinders University, Bedford
- 13 Park, Australia.
- 14 * Address correspondence to: <u>nicholas.eyre@adelaide.edu.au</u> (N.E.) and
- 15 <u>michael.beard@adelaide.edu.au</u> (M.B.)
- 16 1 N.S.E. and S.M.J. contributed equally to this work.
- ¹⁷ ² Current address: The Australian Wine Research Institute, Glen Osmond, South Australia,
- 18 Australia.
- ³ Current address: Department of Microbiology, Monash University, Clayton, Victoria,
- 20 Australia
- 21 Keywords: dengue virus, NS1, mutagenesis, virus replication, virus assembly, electron
- 22 microscopy
- 23 Running Title: Mutational analysis of dengue virus
- 24 Abstract Word Count: 225 words. Importance Word Count: 148 words. Main Text Word
- 25 Count (excluding References and Figure Legends): 8498 words.

1

Downloaded from http://jvi.asm.org/ on September 29, 2017 by UNIVERSITY OF EXETER

26 ABSTRACT

Dengue virus (DENV) is a major global pathogen that causes significant morbidity and 27 mortality in tropical and sub-tropical areas worldwide. An improved understanding of the 28 regions within the DENV genome and its encoded proteins that are required for the virus 29 replication cycle will expedite development of urgently required therapeutics and vaccines. 30 We subjected an infectious DENV genome to unbiased insertional mutagenesis and 31 employed next-generation sequencing to identify sites that tolerate 15-nucleotide insertions 32 during the virus replication cycle in hepatic cell culture. This revealed that regions within 33 capsid, NS1 and the 3'UTR were most tolerant of insertions. In contrast, prM- and NS2A-34 encoding regions were largely intolerant of insertions. Notably, the multifunctional NS1 35 protein readily tolerated insertions in regions within the Wing, connector and β -ladder 36 domains with minimal effects on viral RNA replication and infectious virus production. 37 Using this information we generated infectious reporter viruses, including a variant encoding 38 39 the APEX2 electron microscopy tag in NS1 that uniquely enabled high resolution imaging of 40 its localization to the surface and interior of viral replication vesicles. Additionally, we generated a tagged virus bearing an mScarlet fluorescent protein insertion in NS1 that, 41 42 despite an impact on fitness, enabled live cell imaging of NS1 localization and traffic in infected cells. Overall, this genome-wide profile of DENV genome flexibility may be further 43 dissected and exploited in reporter virus generation and antiviral strategies. 44

45

46 **IMPORTANCE**

47 Regions of genetic flexibility in viral genomes can be exploited in generation of reporter 48 virus tools and should arguably be avoided in antiviral drug and vaccine design. Here we 49 subjected the DENV genome to high-throughput insertional mutagenesis to identify regions 50 of genetic flexibility and enable tagged reporter virus generation. In particular, the viral NS1

protein displayed remarkable tolerance of small insertions. This genetic flexibility enabled 51 52 generation of several novel NS1-tagged reporter viruses, including an 'APEX2'-tagged virus that we employed in high resolution imaging of NS1 localization in infected cells by electron 53 microscopy. For the first time this analysis revealed the localization of NS1 within viral 54 55 replication factories known as 'vesicle packets' (VPs), in addition to its acknowledged localization to the luminal surface of these VPs. Together this genetic profile of DENV may 56 be further refined and exploited in identification of antiviral targets and generation of reporter 57 virus tools. 58

60 **INTRODUCTION**

Dengue virus is a mosquito-borne flavivirus that causes approximately 100 million symptomatic infections and 25,000 deaths each year (1). No antiviral drugs are available and the only approved vaccine is partially limited in efficacy, is only available in certain countries and is not recommended for young children or the elderly (2). Accordingly, there remains an urgent need for development of safe and effective antiviral therapies and vaccines; challenges that are made more difficult by significant gaps in our understanding of the precise functions of the individual viral proteins and their domains.

68 Following entry into susceptible cells via clathrin-dependent endocytosis, the plus-69 strand RNA viral genome of DENV is released into the cytosol and translated by the host ribosome machinery at the rough endoplasmic reticulum (ER). The encoded polyprotein is 70 71 then proteolytically cleaved co- and post-translationally by host and viral proteases to liberate the individual structural proteins capsid, prM and E and the non-structural (NS) proteins NS1, 72 NS2A, NS2B, NS3, NS4A, NS4B and NS5. The NS proteins are essential for replication of 73 the viral genome via a negative-strand RNA intermediate in virus-induced membranous 74 75 organelles know as replication factories (3). Specifically, viral RNA replication mediated by the RNA-dependent RNA-polymerase NS5 is thought to take place within invaginations of 76 the ER membrane known as vesicle packets (VPs), while pores in these VPs may enable 77 exchange of metabolites and export of newly synthesised genomes for encapsidation (4). 78 Accordingly, virus particle assembly is thought to take place in close proximity to VP pores 79 and virus particles can be observed by electron microscopy (EM) in ordered arrays that are 80 encased by 'virion bags' at these sites (4). The other major morphotype of DENV-induced 81 membrane rearrangements are convoluted membranes (CMs), which are drastic 82 rearrangements of ER membranes that are thought to serve polyprotein expression and 83 maturation and may also serve as membrane reservoirs for further VP biogenesis (4, 5). 84

While NS4A may be principally required for these rearrangements (6), other NS proteins are 85 also likely to be involved. NS proteins, such as NS1, NS2A and NS3, also play essential roles 86 in virus particle production, possibly by co-ordinating budding of newly formed 87 nucleocapsids into the ER lumen and their envelopment with membranes that are enriched 88 with the structural proteins prM and E (7-10). The conventional secretory pathway is then 89 exploited in the release of virions, which involves a number of post-translational 90 modifications of structural proteins that confer infectivity to virus particles, including 91 cleavage of prM by the host protease furin in the *trans*-Golgi network (TGN) (11). 92

Reverse genetics analyses have been essential for our current understanding of the 93 DENV replication cycle and the functions of the individual viral proteins and RNA elements. 94 95 However, these studies are laborious and time consuming and are therefore typically limited 96 to the analysis of discrete regions of a viral genome and/or encoded protein in a single study. One approach to overcome this bottleneck involves the combination of high-throughput 97 random mutagenesis of a cloned viral genome with next generation sequencing (NGS) to 98 quantify the degree to which regions within viral genomes tolerate mutations in cell culture 99 models of viral replication. This approach has recently been employed to provide global maps 100 of genetic flexibility for viruses such as hepatitis C virus (HCV), influenza A virus (IAV) and 101 measles virus (MeV) and how this genetic flexibility or inflexibility relates to functions of 102 viral proteins and their targeting by host immune responses (12-16). Here, we have combined 103 transposon-mediated random insertional mutagenesis and NGS to generate a global map of 104 genetic flexibility for a cloned DENV serotype 2 genome (DENV-2; strain 16881). We reveal 105 106 for the first time that capsid- and NS1-encoding regions and the 3'UTR display the greatest overall genetic flexibility. In particular, NS1 was highly tolerant of insertions in regions 107 108 surrounding N-glycosylation sites in the Wing and β -ladder domains and in a region surrounding a site in the second *connector* domain that is N-glycosylated for several other 109

5

lournal of Virology

flaviviruses. In contrast other regions such as those encoding prM and NS2A were highly 110 intolerant of insertions. Building on these insights, we then generated a panel of infectious 111 epitope- and reporter-tagged DENV-2 isolates, including a variant encoding the APEX2 EM 112 reporter in NS1 that enabled high resolution imaging of NS1 at the membrane and interior of 113 VPs and, less strongly, at the Golgi and modified ER membranes. We also generated a novel 114 115 DENV2 derivative encoding an mScarlet fluorescent protein insertion in NS1 that enabled visualization of NS1-mScarlet localization and traffic in infected cells and revealed that 116 intense juxtanuclear NS1 foci are relatively static while small and weakly fluorescent 117 structures frequently display rapid, long-range, bidirectional traffic. Together, our data 118

> provide new insights into the localization and traffic of NS1 and provide a resource that may 119 be exploited in future generation of tagged reporter viruses and in development of antiviral 120 121 strategies directed towards genetically inflexible regions of the DENV genome and encoded proteins. 122

123

RESULTS 124

High-throughput transposon mutagenesis coupled to NGS reveals regions of genetic 125 flexibility within the DENV-2 genome. We subjected a cloned DENV-2 genome (strain 126 16681) to random transposon mutagenesis using Mu transposase to generate a mutant pool 127 comprised of approximately 250,000 plasmid clones. The transposon body encoding a 128 kanamycin resistance cassette was then excised and the plasmid pool re-ligated to generate 129 the final mutant pool comprised of a similar number of plasmid clones, each bearing a single 130 15-nucleotide (nt) insertion of which 10-nt are transposon-derived (5'-TGCGGCCGCA-3') 131 and 5-nt are duplicated from the target site. When inserted in a coding region of the genome, 132 133 this results in a 5 amino acid insertion whose sequence is dependent on the frame and insertion site (C-G-R-I/M/T/N/K/S/R, L/M/V-R-P-H/Q or X-A-A-A). From this mutant 134

large scale electroporation of Huh-7.5 hepatoma cells. Following culture of electroporated 136 cells for 6 days, total cell RNA was extracted from remaining cell monolayers (Pool 1: 137 'Replication-competent'), and cell culture supernatants were collected, clarified and applied 138 to naïve cells. Infected target cells were then cultured for 2 days before extraction of total cell 139 RNA to generate Pool 2: 'Infectious' (Fig. 1A). Immunofluorescence microscopy analysis of 140 parallel cell cultures confirmed robust DENV-2 replication in these cultures and an expected 141 delay in replication and spread of the mutant pool as compared to wildtype DENV-2 (not 142 shown). Total RNA from each pool was then subjected to RT-PCR using DENV-specific 143 primers that covered the genome in six overlapping fragments. In parallel, this PCR was also 144 145 performed to determine insertion distribution in the initial mutant plasmid pool. NGS 146 libraries for each pool were prepared using Nextera XT (Illumina) and sequenced on the NextSeq500 platform. Sequence reads were mapped to the reference DENV-2 genome and 147 the frequency of transposon insertions at each position was measured for each pool (Fig. 1 148 and Dataset S1). This revealed that insertions were generally evenly distributed across the 149 DENV-2 genome in both the mutant plasmid pool (not shown) and the mutant DENV-2 RNA 150 library, Pool 0, used for transfection (Figs. 1B), with the exception of 'hotspots' for insertions 151 in the NS2A-encoding region that may relate to disruption of cryptic bacterial promoter-152 153

135

driven expression or activity of toxic genes that otherwise limit propagation of flavivirus clones in bacteria (17). In total 74.2, 71.4, 59.2 and 63.4 million reads were generated for the plasmid pool, Pool 0, Pool 1 and Pool 2, respectively, while digital counting of transposon insertions revealed 7867, 4700, 1122 and 1003 unique insertions in the DENV2 genome for these respective pools.

plasmid pool we generated in vitro transcribed viral RNA, referred to as Pool 0: 'Input', for

We compared genome insertion counts in the initial input mutant pool (Pool 0; Fig.
1B) with those capable of viral RNA replication (Pool 1; Fig. 1C) and those capable of viral

160

and NS1-encoding regions and the 3'UTR were most tolerant of 15-nt insertions, whereas 161 other regions such as prM- and NS2A-encoding regions were largely intolerant of these 162 insertions. Fig. 1E shows insertions that were most strongly selected against (cyan peaks), 163 and insertion mutants capable of being sustained during viral RNA replication but not 164 165 infectious virus production (blue and magenta peaks). All other peaks, and particularly vellow and red peaks, represent insertion mutants that are viable throughout the entire viral 166 life cycle. We also assessed the frequency of insertions in replication-competent and 167 infectious pools (Pools 1 and 2, respectively) as a percentage of those counted in the initial 168 input pool (Pool 0) and this normalised view also highlighted sites in capsid- and NS1-169 170 encoding regions that were most tolerant of insertions and, in particular, the high sensitivity of prM- and NS2A-encoding regions to insertions (Fig. 2). In this context, the encoded amino 171 172 acid sequences of the 25 most-tolerated insertions are displayed in Dataset S1. More detailed analysis is clearly required before firm conclusions can be drawn as to which frame-173 dependent transposon-encoded peptide sequences are better tolerated at different sites within 174 the viral proteins. Nevertheless, of the 25 most-tolerated insertions, 60% (15/25) encoded C-175 G-R-I/M/T/N/K/S/R insertions, 28% (7/25) encoded X-A-A-A insertions and only 12% 176 (3/25) encoded L/M/V-R-P-H/Q insertions (Dataset S1, column 'N'), highlighting that the 177 impact of a 5 a.a. insertion at a given site can be strongly influenced by factors such as the 178 charge, hydrophobicity and bulkiness of the inserted peptide. Given the high degree of 179 overlap between Pool 1 and Pool 2, it is likely that spread of infectious virus during the 6 day 180 culture period following electroporation of the mutant library strongly contributed to 181

RNA replication and infectious virus production (Pool 2; Fig. 1D). This revealed that capsid-

representation of infectious mutant viruses in Pool 1. This possibility is also consistent with

the unexpected selection against regions encoding structural proteins that are not required for

viral RNA replication in Pool 1 (Figs. 1C and 2B).

8

near the termini of viral proteins, for example at the C-terminus of capsid, E, NS1 and NS2B 186 proteins, at the N-terminus of NS3 and at both N- and C-termini of NS4B (Fig. 1E and Fig. 187 2B). Provided that the sites of DENV polyprotein cleavage are not disrupted by these 188 insertions, the propensity of viral proteins to better tolerate insertions at their termini is 189 190 consistent with a reduced likelihood of such insertions to disrupt the overall structure and inturn interactions and functions of these viral proteins. Furthermore, for the coding portion of 191 192 the genome, regions that were most tolerant of insertions were generally less strongly conserved between different DENV serotypes and other flaviviruses, although these regions 193 were not characterized by unusually long stretches of sequence variation when the amino acid 194 195 sequences of different flaviviruses were aligned and compared (Fig. S1). Given that compact 196 viral genomes rarely maintain non-functional or non-essential sequences, regions that are highly tolerant of insertions may play roles in immune evasion, pathogenesis or virus-host 197 198 interactions that are not re-capitulated in Huh-7.5 cell culture.

It was also apparent that peaks representing tolerated mutations were often observed

199

185

DENV NS1 protein is highly tolerant of small insertions in regions surrounding N-200 glycosylation sites. Of the DENV proteins, the multifunctional NS1 protein showed the 201 202 greatest tolerance to transposon insertions in the context of the complete infectious virus replication cycle. Closer examination of the sites that tolerated insertions, with respect to the 203 recently solved crystal structure of NS1 (18), revealed that sites within the second half of the 204 205 Wing domain, in the second *connector* and in the N-terminal region of the β -ladder domain 206 were most tolerant of transposon insertions, while sites near the C-terminus of the β -ladder were moderately tolerant of insertions (Fig. 3A). In contrast, the N-terminal β -roll domain, 207 the first half of the Wing domain and the first connector that separates these domains were 208 highly sensitive to transposon insertions, consistent with a recent alanine scanning 209

Accepted Manuscript Posted Online

lournal of Virology

mutagenesis study that identified several replication-lethal mutations in these domains, 210 211 including C4A, W8A, Y32A, C55A and R62A (8). Notably, the regions that were most tolerant of insertions were clustered in close proximity to the N-glycosylation sites in the 212 Wing and β -ladder domains, Asn-130 and Asn-207, respectively, and surrounding a site in 213 214 the second *connector* domain (Gln-175) that is a glycosylated Asn residue for several other flaviviruses, including West Nile virus (WNV), Saint Louis encephalitis virus (SLEV) and 215 216 Murray Valley encephalitis virus (MVEV) (19). As N-glycosylation of NS1 is likely to be 217 important to its functions as a secreted hexameric lipoparticle that modulates immune responses and causes vascular leakage, insertions in the regions surrounding these N-218 glycosylation sites may impact upon functions of secreted NS1 in immunomodulation and 219 220 vascular leakage that are not recapitulated in hepatoma cell culture.

To better understand the location of tolerated transposon insertions as they relate to 221 222 the three-dimensional structure of NS1 dimers, we visualised the locations of the 10 most 223 tolerated insertion sites (Pool 2 / Pool 0) in the crystal structure of DENV-2 NS1 dimer 224 (PDB: 406B), provided that at least two positions in the given codon preceded tolerated 225 insertions (Fig. 3B). This approach, focussing on sites that tolerated insertions in at least two 226 alternative codon positions and hence resulted in alternative encoded peptide insertions (C-G-227 R-I/M/T/N/K/S/R, L/M/V-R-P-H/Q or X-A-A-A), was employed to highlight sites that were 228 broadly tolerant of small insertions. This revealed that the sites most tolerant of insertions 229 were predicted to be solvent-exposed and distant from the lipid bilayer-interacting inner hydrophobic face of the β -roll domain and adjacent 'greasy finger' loop (18). The two 230 231 residues that preceded the most tolerated insertions were Lys-174 (~550-fold enrichment from input) and Thr-126 (~93-fold enrichment from input) and these sites were flanked by 232 several other top-ranking tolerated insertion sites, including Glu-174 (~81-fold), Asn-130 233 234 (~75-fold), Ser-125 (~64-fold), Ser-128 (~58-fold) and Glu-127 (~44-fold).

Another region in the DENV-2 genome that was broadly tolerant of insertions was the 235 236 capsid-encoding region, although the degree to which insertions were tolerated was 237 considerably lower than that of NS1 (see Fig. 2). Capsid is the least conserved of the flavivirus proteins, although its general structural properties and charge distribution are well-238 conserved. Structural studies of this highly basic protein have shown that the capsid monomer 239 contains four α -helices (α 1 to α 4), while the dimer has an asymmetric charge distribution 240 241 such that the highly basic $\alpha 4$ - $\alpha 4$ ' region may interact with viral RNA while the hydrophobic cleft, comprised of $\alpha 1 - \alpha 1$ and $\alpha 2 - \alpha 2$ regions, on the opposite side of the molecule forms an 242 243 apolar surface that is predicted to interact with membranes (20, 21). Examination of the 244 location of tolerated insertions revealed that the C-terminus of capsid towards the end of the 245 α 4 region and, in particular, the region immediately downstream of the NS2B/3 cleavage site and adjacent to the transmembrane anchor were most tolerant of insertions (Fig. 4). 246 Additionally the region surrounding the $\alpha 1$ region was broadly and moderately tolerant of 247 insertions, consistent with the flexibility of this region implied by the differing orientations of 248 DENV and WNV $\alpha 1$ and mutational studies demonstrating that substitutions of uncharged 249 250

amino acids in the α 1 helix and α 1- α 2 connecting loop do not impair DENV propagation (22, 23). In contrast, the N-terminus of capsid and the α 2 and α 3 regions were more sensitive to insertions. Taken together, the high tolerance of capsid for insertions is consistent with it being the least conserved of the flavivirus proteins.

254

The influence of host cell type and species on the sensitivity of DENV-2 to 15-nt transposon insertions. To investigate how host cell type and species impacts upon the tolerance of DENV-2 to transposon-derived 15-nt insertions, the infectious virus-containing cell culture supernatant from Huh-7.5 cells that were transfected with RNA transcripts for the mutant DENV-2 RNA library was applied in parallel to naïve mammalian cell lines Huh-7.5

and Vero cells and the insect C6/36 cell line. At 48 hours post-infection RNA was then 260 extracted from these cells and subjected to RT-PCR for Illumina sequencing (Fig. 5A). The 261 frequency of 15-nt transposon insertions was measured and compared for DENV-2 genomes 262 recovered from infected Huh-7.5, Vero and C6/36 cells (Fig. 5B-D), employing an overlay of 263 the respective maps to highlight which transposon insertions are differentially tolerated in the 264 265 alternative host cell types (Fig. 5E). Despite the appreciable differences in infection rates for revealed by parallel immunofluorescent staining of infected cells (Fig. 5F), our analysis 266 revealed very close overlap between regions that displayed tolerance of insertions in the 267 DENV-2 genome in these highly divergent host cells (Fig. 5E). However, subtle but clear 268 differences were apparent (see Dataset S1), including modest increases in the frequency of 269 270 tolerated transposon insertions in the 3'-UTR and sites within E for C6/36 host cells as compared to Huh-7.5 and Vero host cells (see yellow peaks for Fig. 5E). In contrast, C6/36 271 272 host cells were associated with modest decreases in the frequency of tolerated insertions in regions surrounding the Asn-207 glycosylation site in NS1 and in the C-terminus of NS2B 273 (see blue peaks for Fig. 5E). Taken together these experiments indicate that, following initial 274 selection in Huh-7.5 human hepatoma cells, host cell selective pressures do not dramatically 275 alter regions of genetic flexibility within the DENV-2 genome. 276

277

Generation of tagged reporter viruses to study the DENV replication cycle and viral protein localization and interactions. Epitope- and reporter-tagged viruses are valuable tools to study viral protein localization and interactions in the context of productive viral infections. However, their development is challenging and requires prediction of sites that may tolerate insertions and empirical testing of candidate tagged viruses. Guided by our transposon mutational profile of sites that tolerate 15-nt (5 a.a.) insertions in the DENV2 genome, we generated and tested a panel of epitope- and reporter-tagged DENV-2 constructs, 285

286 insertions and their essential but incompletely understood functions in the viral replication cycle (Fig. 5A). We found that the region at the C-terminus of the capsid pre-cursor and 287 adjacent to the transmembrane anchor region ('CAPmem'), following Gly-103, could readily 288 289 tolerate small epitope tags. This included the recently developed NanoBiT luciferase 290 complementation component SmBiT (11 a.a.) for use in studying protein-protein interactions 291 in living cells (24), and the split fluorescent protein component GFP11 (16 a.a.) for use in live cell imaging in cells expressing the complementary GFP 1-10 fragment (25). Tolerance 292 293 of this site for insertions was influenced by the overall charge of the inserted peptide as incorporation of the smaller but highly charged FLAG tag at this site severely attenuated viral 294 295 replication and spread (results not shown). We also generated tagged viruses encoding FLAG or GFP11 epitope tag insertions within NS1 between Lys-174 and Gln-175 (Fig. 6A). 296 297 Similarly, we generated virus constructs bearing insertions of the larger APEX2 EM tag (26, 27) or the extremely bright NanoLuc (NLuc) luciferase reporter (28) at this same site in NS1. 298 Western blot analysis of Huh-7.5 cells transfected with the respective tagged DENV-2 299 or wildtype DENV-2 RNA transcripts revealed ready detection of NS1 for all virus constructs 300 and expected increased molecular weights of tagged NS1 proteins (Fig. 6B). We also noted a 301 moderate increase in the levels of tagged NS1 protein that may reflect minor effects of tag 302 insertions at this site on NS1 stability. Importantly, however, analysis of NS1 protein levels 303 in cell culture supernatants revealed no major tag-associated defects in NS1 secretion (Fig. 304 6B), although further analysis is required to definitively clarify whether the efficiency and 305 306 kinetics of NS1 secretion are altered. Analysis of the replicative fitness of these tagged viruses compared to wildtype DENV-2 revealed that DENV2-NS1-FLAG displayed wildtype 307 308 levels of viral replication and spread, as determined by automated immunofluorescence analysis (Fig. 6C), and wildtype levels of infectious virus production (Fig. 6D). Similarly, 309

specifically focussing on the NS1 and capsid proteins given their high degree of tolerance of

Z

viruses bearing GFP11 or SmBiT insertions adjacent to the capsid membrane anchor or a 310 GFP11 insertion in NS1 displayed robust replication and spread and infectious virus 311 production that was only moderately impaired compared to wildtype DENV2 (Fig. 6C-D). 312 While viruses encoding larger APEX2 (783-nt, ~28 kDa) or NLuc (516-nt, ~19 kDa) 313 insertions in NS1 were appreciably attenuated compared to wildtype DENV-2, they 314 315 nonetheless displayed robust levels of viral replication and infectious virus production (Fig. 6C-D), supporting their utility in detailed analysis of NS1 localization, using DENV2-NS1-316 317 APEX2, and highly sensitive and simple monitoring of protein levels, using DENV2-NS1-318 NLuc (see below). Interestingly, the tolerance of insertions at this site in NS1 appears to be 319 highly dependent on the sequence and/or structure of the inserted protein as several other 320 reporter protein insertions at this site were not tolerated, including those of green fluorescent protein (GFP) and the self-labelling SNAP-tag (results not shown). 321

Given the potential for tag insertions to alter NS1 conformation, glycosylation, 322 secretion and localization, we further investigated these properties for our panel of epitope-323 and reporter tagged DENV-2 derivatives. Firstly, in our hands non-reducing, non-denaturing 324 conditions were required for reactivity of the anti-NS1 mAb 4G4 towards secreted DENV-2 325 NS1 (Fig. 7A), with results suggesting that the native epitope recognised by this antibody is 326 similarly retained for all NS1-tagged viruses. Furthermore, we assessed whether N-327 glycosylation of NS1 is affected by the presence of tag insertions in NS1 by digesting cell 328 culture supernatants with PNGase F prior to Western blotting (Fig. 7B). This revealed a 329 similar shift in the apparent molecular weight of wildtype and tagged NS1 proteins, 330 indicating no major defects in N-glycosylation of NS1-tagged variants. Given the potential 331 for cell type- and/or species-specific effects on the replicative fitness of these tagged viruses, 332 333 we also compared infectious virus production for wildtype and tagged viruses following viral RNA transfection of Aedes albopictus-derived C6/36 cells and African green monkey-derived 334

Vero cells (Fig. 7C-D). Consistent with observations in Huh-7.5 cells (Fig. 6D), in both 335 C6/36 and Vero cells DENV2-NS1-FLAG produced wildtype levels of infectious virus 336 production, other small insertions in capsid (SmBiT and GFP11) and NS1 (GFP11) were 337 associated with moderate impairment of infectious virus levels and larger insertions in NS1 338 (APEX2 and NLuc) were associated with more marked reductions in infectious virus levels 339 340 (Fig. 7C-D). Importantly all tagged viruses outlined in Fig. 6 displayed unaltered localization of NS1 and capsid proteins in Huh-7.5 cells and minimal changes to the degree of their 341 colocalization with dsRNA, a marker of viral replication factories (Fig. 8). Taken together, 342 this panel of infectious tagged viruses, and future tagged viruses that are rationally generated 343 using the insertional mutation map of DENV-2 as a guide, will serve as important tools to 344 345 study viral protein localization, traffic and interactions in the context of a productive viral 346 infection.

347

Sensitive luminescence-based monitoring of intracellular and secreted NS1 protein 348 levels. We next explored the utility of the DENV2-NS1-NLuc virus in monitoring 349 intracellular and secreted NS1 protein levels during viral infection in cell culture. For this, 350 Huh-7.5 cells in 96-well plates were infected with serial dilutions of DENV2-NS1-NLuc, 351 washed and returned to culture for 48 h prior to determination of extracellular and 352 intracellular NS1-associated NLuc activity (Fig. 9A). This revealed simple and extremely 353 sensitive detection of NS1-NLuc levels over a large dynamic range (~4 orders of magnitude). 354 As expected, extracellular NS1-NLuc was also strongly detected with levels closely reflecting 355 those of intracellular NS1-NLuc. Furthermore, we confirmed the utility of this luminescent 356 virus in antiviral drug testing by measuring the impact of the recently identified pan-flaviviral 357 358 inhibitor Nanchangmycin on viral infection and replication (29). Consistent with that study, Nanchangmycin pre-treatment for 1 hour was associated with dose-dependent inhibition of 359

virus encoded NS1-NLuc, measured in both intracellular and extracellular samples at 48 h.p.i.
(Fig. 9B). Taken together, DENV2-NS1-NLuc enables sensitive monitoring of NS1 protein
levels during viral infection and may be well-suited to high-throughput screening.

363

High resolution imaging of NS1 localization using APEX EM and STED super-364 365 resolution microscopy. Early studies using immuno-EM revealed the localization of NS1 to vesicle packets in DENV-infected cells and its co-localization with dsRNA at these sites (30), 366 consistent with the essential role of NS1 in viral genome replication. Furthermore, recent 367 studies demonstrated co-localization and interaction of NS1 with capsid and E proteins at 368 putative viral assembly sites and/or assembled virions (8). However, traditional antibody-369 370 based approaches are limited in their ability to examine protein localization at high resolution in the context of clear visualization of cellular membranes and, accordingly, many details 371 372 about the exact nature of NS1 localization remain unclear. We therefore examined NS1 localization by APEX EM, which allows high resolution imaging of tagged protein 373 localization by EM while maintaining excellent ultrastructural preservation (26, 27). For this, 374 Huh-7.5 cells were infected with untagged DENV-2 or DENV2-NS1-APEX2 (MOI: ~0.01) 375 or mock-infected and returned to culture for 4 days prior to fixation, labelling with 376 DAB/H₂O₂ and processing for EM. Brightfield microscopy following DAB/H₂O₂ labelling 377 confirmed strong and specific staining of NS1 that was unique to DENV2-NS1-APEX2-378 infected cells (Fig. 10A). Samples were subsequently labelled with electron-dense OsO₄, 379 which stains the osmiophilic DAB polymer, and further processed for EM. As observed in 380 381 standard EM analysis of DENV-infected cells, untagged virus infection was associated with typical induction of CMs and VPs that were clearly but not intensely stained (Figs. 10B-i and 382 383 10B-ii respectively), and were absent in mock-infected cells (not shown). In contrast, in cells that were infected with DENV2-NS1-APEX2, intense staining of NS1-APEX2 could be 384

observed in clusters of VPs, with somewhat diffuse staining localized to the outer membrane 385 of VPs and intense, tightly localized staining of punctae that were asymmetrically distributed 386 within VPs (Fig. 10B-iv). We also observed clear but less intense staining of ER membranes 387 that in many instances were proximal to lipid droplets (Fig. 10B; iv). This approach also 388 revealed clear staining of NS1-APEX2 in the Golgi (Fig. 10B; iii). While we could not 389 390 clearly discern virus particles in these cells, we observed occasional examples of intensely stained clusters adjacent to VPs (Fig. 10B; v) and NS1-APEX2-positive highly ordered arrays 391 392 (Fig. 10B; vi) that may be relevant to the function(s) of NS1 in virus particle assembly and 393 secretion (8). Although we observed no unanticipated effects of the APEX2 insertion on NS1 394 protein processing (Fig. 6B), secretion (Figs. 6B and 7A), glycosylation (Fig. 7B) or 395 localization (as determined by confocal microscopy; Fig. 8A), given the reduced fitness of the DENV2-NS1-APEX2 virus further studies using complementary imaging techniques are 396 required to support our findings regarding NS1 localization using APEX EM. 397

In this context, to complement the APEX EM imaging analysis of NS1 localization 398 we also applied the DENV2-NS1-FLAG recombinant virus, which encodes a single FLAG 399 tag within NS1, to STimulated Emission Depletion (STED) super-resolution imaging of the 400 localization of FLAG-tagged NS1 and dsRNA, given that this virus displayed wildtype levels 401 of replication and infectious virus production and enables particularly strong and specific 402 labelling of NS1-FLAG, with anti-FLAG antibodies, in combination with anti-dsRNA 403 labelling. While NS1-FLAG and dsRNA displayed near-complete co-localization when 404 imaged by standard laser scanning confocal microscopy (Fig. 8A), even when image 405 deconvolution was applied (Fig. 11A), STED imaging in combination with deconvolution 406 revealed that dsRNA foci were frequently immediately adjacent to NS1 foci, which displayed 407 408 a more reticular localization pattern compared to the intense and largely discrete dsRNA foci (Fig. 11B). Taken together, these experiments clarify the localization of NS1 with respect to 409

Σ

VPs and provide powerful new tools to further examine NS1 localization as it relates to its
roles viral RNA replication, virus particle production and as a secreted mediator of immune
evasion and pathogenesis.

413

Live cell imaging of mScarlet-tagged NS1. Although the GFP11-tagged viruses, DENV2-414 415 CAPmem-GFP11 and DENV2-NS1-GFP11, displayed robust viral replication and infectious virus production, we could not reliably detect strong GFP11-associated fluorescence upon 416 complementation with heterologously expressed GFP(1-10) (Eyre NS, Beard MR; 417 unpublished results). This may be attributable to inefficient fluorescence complementation 418 and/or inaccessibility of the incorporated GFP11 peptides to GFP(1-10); obstacles that may 419 be overcome by development of analogous viruses bearing multiple tandem repeats of 420 GFP11, targeting of GFP(1-10) to the ER lumen and/or application of newly developed split 421 422 fluorescent protein systems based on GFP11/GFP(1-10) with improved complementation efficiencies (25, 31). Therefore, while our GFP11-tagged viruses provide important proof-of-423 concept that capsid and NS1 proteins can tolerate small functional insertions designed for 424 fluorescent imaging, further optimization is required to improve their utility in demanding 425 applications such as live cell imaging. We therefore developed a novel DENV-2 construct 426 featuring an extremely bright and monomeric red fluorescent protein, mScarlet (32), inserted 427 within NS1 (Fig. 12A). This recombinant virus supported infectious virus production and 428 dictated strong NS1-associated fluorescence (Fig. 12B), despite appreciable attenuation 429 compared to wildtype DENV-2 (Fig. 12C). We next investigated NS1 localization and traffic 430 by live cell imaging analysis of Huh-7.5 cells transfected with DENV2-NS1-mScarlet RNA 431 transcripts. At 6 days post-transfection NS1-mScarlet fluorescence was observed throughout 432 433 the entire culture (Fig. 12D), while imaging at high magnification revealed characteristic localization of NS1-mScarlet to large, intensely labelled juxtanuclear foci and smaller, 434

weakly fluorescent foci throughout the cytoplasm (Fig. 12E). Live cell imaging over 5 minute 435 periods revealed that the intensely labelled NS1-mScarlet foci were largely static (Fig. 12E, 436 cyan arrows and Movie S1), while a minority of small and weakly fluorescent foci displayed 437 rapid, long-range bidirectional traffic that is characteristic of microtubule-dependent transport 438 (Fig. 12E, cyan arrowheads and Movie S1). Importantly, similar NS1-mScarlet localization 439 440 and trafficking patterns were observed for cells infected with DENV2-NS1-mScarlet, including in longer-term (~45 minute) live cell imaging acquisitions (Movie S2). Taken 441 together these results and the DENV2-NS1-mScarlet virus provide the basis for more detailed 442 analysis of NS1 localization and traffic in live infected cells and indicate that intense NS1 443 foci that likely represent replication complexes are relatively static, while weakly fluorescent 444 NS1 foci that may be involved in other aspects of the viral replication cycle can display rapid 445 long-range traffic. Further characterization of the DENV2-NS1-mScarlet recombinant virus 446 and development of adapted variants that closely mirror the replication, infectious virus 447 production and NS1 secretion kinetics of wildtype DENV2 will enable detailed analysis of 448 NS1 localization, traffic and interactions with relevant viral and host cell factors during a 449 450 productive infection.

451

452 **DISCUSSION**

453 Reverse genetics studies have contributed greatly to our understanding of the DENV 454 replication cycle and the functions of the individual viral proteins and genetic elements. 455 However, these studies are highly laborious and are typically limited to analysis of discrete 456 regions of individual viral proteins. Our study employed random transposon mutagenesis and 457 high-throughput sequencing to provide a global overview of regions of genetic flexibility 458 within the DENV-2 genome and its encoded proteins. This data provides a resource 459 identifying genetically flexible regions that should arguably be avoided in antiviral and

Accepted Manuscript Posted Online

lournal of Virology

lournal of Virology

vaccine development strategies, as these sites may be prone to escape mutations with minimal 460 impact on viral replicative fitness. Conversely, sites that are broadly tolerant of insertions can 461 be exploited in the generation of infectious epitope- and reporter-tagged viruses. These 462 viruses can be employed in advanced applications such as high-resolution imaging and 463 interrogation of protein-protein interactions. 464

465 Our transposon mutagenic profile of DENV2 genetic flexibility indicates that the regions encoding prM, NS2A and NS4A are highly intolerant of 15-nt insertions. For NS2A, 466 467 an eight-transmembrane protein with essential roles in viral RNA replication and infectious virus production, our observations of intolerance to insertions are consistent with recent 468 alanine scanning mutagenesis studies that have revealed numerous mutations, particularly in 469 470 transmembrane regions, that are lethal to viral RNA replication or infectious virus production (9, 10). Similarly, recent site-directed mutagenesis studies of NS4A, which is essential for 471 472 DENV-induced membrane rearrangements, have identified numerous conserved residues that are required for its oligomerization and viral RNA replication (33, 34). However, the lack of 473 detection of replication-competent (Pool 1) viruses bearing insertions in the prM-encoding 474 region was more surprising as this region has no known involvement in viral RNA 475 replication. Whilst it is possible that spread of infectious virus in Pool 1 has masked the 476 presence of replication-competent prM mutants, it is also possible that insertion mutations 477 within this region have unexpected dominant-negative effects on viral replication. Further 478 studies are required to explore the apparent impact of prM mutations on DENV replication. 479

Overall, the regions encoding capsid, NS1 and the 3'-UTR were most tolerant of 15-480 nt insertions. As discussed above, capsid is the least conserved of all flavivirus proteins, 481 although its charge distribution is strongly conserved and structural features are highly 482 483 similar for capsid proteins of different flaviviruses (22). Accordingly, its relatively high tolerance for 15-nt insertions is not unexpected, especially for insertions that minimally alter 484

Ĕ T	485	its overall charge. In this context, none of the possible insertions encode negatively charged
	486	peptides (C-G-R-I/M/T/N/K/S/R, L/M/V-R-P-H/Q or X-A-A-A). Similarly, Region I of the
	487	3'UTR, where transposon insertions are most tolerated, is the most variable of all DENV
	488	nucleotide sequences with various deletions and point mutations identified in mosquito cell-
Accepted Mulluscriptic	489	adapted populations (35, 36). Although moderately conserved across flavivirus species, the
	490	NS1 protein was remarkably tolerant of 15-nt insertions. Largely consistent with a recent
	491	mutagenesis study (8), we found that the N-terminal β -roll, which contains a di-amino acid
	492	motif that may mediate interaction with NS4B and ER membrane association (37), the N-
	493	terminal half of the <i>Wing</i> domain and the C-terminal half of the β -ladder domain were highly
	494	sensitive to insertions. In contrast, relatively broad regions surrounding the N-glycosylation
	495	sites in the Wing (N130) and β -ladder (N207) domains and sites in close proximity to an N-
	496	glycosylation site in the <i>connector</i> domain of other flaviviruses (N175) were highly tolerant
	497	of insertions. Examination of the location of these sites in the crystal structure of the NS1
	498	dimer demonstrated that they were all solvent-exposed and relatively distant from the
	499	putative ER membrane-associating β -roll and greasy finger loop of the β -ladder (18).
	500	Likewise, in the context of the secreted NS1 hexamer these regions of genetic flexibility are
	501	distant from the lipoparticle interior and central lipid core that are contained by six copies of
	502	the β -roll (18). Accordingly, we hypothesise that the regions of high tolerance of insertions
	503	identified in our study are not required for functions of NS1 in viral RNA replication or
	504	infectious virus production but, rather, may be required for extracellular functions of NS1 in
> 1	505	immune evasion and pathogenesis that are not recapitulated in hepatoma cell culture. If so,

interaction with NS4B and ER membrane association (37), the Ndomain and the C-terminal half of the β -ladder domain were highly contrast, relatively broad regions surrounding the N-glycosylation and β -ladder (N207) domains and sites in close proximity to an Nconnector domain of other flaviviruses (N175) were highly tolerant n of the location of these sites in the crystal structure of the NS1 they were all solvent-exposed and relatively distant from the associating β -roll and greasy finger loop of the β -ladder (18). of the secreted NS1 hexamer these regions of genetic flexibility are ele interior and central lipid core that are contained by six copies of gly, we hypothesise that the regions of high tolerance of insertions re not required for functions of NS1 in viral RNA replication or on but, rather, may be required for extracellular functions of NS1 in and pathogenesis that are not recapitulated in hepatoma cell culture. If so, such replication-competent and infectious mutants that lack the immune evasion and vascular 506 permeability functions of wildtype NS1 may potentially be combined and exploited in future 507 508 attenuated vaccine strategies. In this context a live-attenuated Zika virus (ZIKV) strain with engineered mutations to abolish NS1 glycosylation has very recently been shown to protect 509

lournal of Virology

534

mice against virus-induced placental damage and fetal demise (38). Alternatively or 510 additionally, regions of genetic flexibility in NS1 may be inherently flexible to skew humoral 511 immune responses towards these epitopes and away from regions that are susceptible to 512 function-neutralising antibody responses and/or facilitate rapid viral adaptation in alternative 513 host species. Such roles have been suggested for genetically flexible regions of influenza A 514 515 virus (IAV) NS1 protein in similar high-throughput insertional mutagenesis studies (13).

Although our mutant library did not achieve saturation, it nonetheless enabled 516 generation of a comprehensive profile of regions in the DENV-2 genome that are broadly 517 tolerant of small (15-nt) insertions and non-essential for viral RNA replication and infectious 518 virus production in hepatoma cells. In this context, sequencing analysis of the initial mutant 519 DENV-2 RNA pool indicated that ~44% of all possible insertions were present. However, 520 additional transposon insertions frequently emerged in sequencing analysis of the replication-521 competent and infectious virus pools (Pools 1 and 2, respectively), such that the percentage of 522 all possible unique transposon insertions in the DENV-2 genome in our study rose to \sim 49%. 523 Future studies of this nature involving near-saturation mutagenesis will help to resolve gaps 524 in our mutational profile of DENV-2 but will not likely alter the overall appearance of this 525 profile. Furthermore, additional approaches are required to better delineate regions that are 526 essential to viral RNA replication and those that are required uniquely for infectious virus 527 production. For example, blockade of infectious virus spread or parallel comparison of 528 genetic flexibility in an analogous subgenomic replicon could resolve regions in the NS 529 proteins that are required for replication versus those required for infectious virus production. 530 As detailed above, another application of our mutational profile of DENV2 is in the 531 rational generation of epitope- and reporter-tagged viruses. While the viability of such viruses 532 533 is predictably dependent on the size and structure of the insertion, our mutational profile

nonetheless provides a valuable resource for prediction of sites that may tolerate insertions

for advanced imaging, proteomics and molecular applications. For example, our APEX EM 535 analysis indicates that NS1 is localized to both the luminal membrane of VPs and in discrete 536 clusters within VPs, in contrast to longstanding models of replication complexes with respect 537 to VPs, which depict NS1 as an exclusively luminal viral protein. Furthermore, live cell 538 imaging studies using mScarlet-tagged NS1 revealed that intensely labelled NS1 foci, which 539 may reflect clusters of vesicle packets, are relatively static. In contrast, small and less 540 intensely labelled NS1 foci infrequently display rapid bi-directional traffic. Although further 541 investigations are required, including confirmation that NS1 secretion is not perturbed by the 542 543 mScarlet insertion, these motile foci may reflect pools of NS1 that are involved in other functions of NS1 such as virus assembly and as a secreted mediator of vascular damage and 544 immune evasion. Further studies using the NS1-tagged viruses developed in this study and 545 additional variations of these tagged viruses may help to further resolve the localization, 546 traffic, interactions and functions of this enigmatic multifunctional viral protein. 547

The transposon mutagenesis-coupled high-throughput sequencing approach applied to 548 DENV-2 here also provides a basis for numerous additional extensions that could rapidly 549 improve our understanding of flavivirus- and host cell-specific functions of viral proteins and 550 genetic elements. For example, this approach could be readily applied to other DENV 551 serotypes, related flaviviruses or alternative cell types to unveil flavivirus- and host cell type-552 and species-specific differences in the functions and interactions of viral proteins. In this 553 context, our analysis of cell type- and/or species-specific determinants of genetic flexibility 554 indicate that the diverse host cells that we examined do not impart markedly different 555 selective pressures that alter the relative fitness of viable transposon mutants. Nevertheless, it 556 is possible that continued passage of the transposon mutant pool in these different cell types 557 558 may further unveil regions of the DENV-2 genome that are differentially susceptible to host cell-specific selective pressures. In regards to flavivirus-specific determinants of viral 559

560

transposon mutagenesis of a cloned ZIKV genome on viral replication and infectious virus production (39). Largely consistent with our findings for DENV-2, Fulton et al demonstrated that NS1 and the structural genes of ZIKV displayed the greatest overall flexibility, although key differences in the mutational maps of DENV-2 and ZIKV were apparent. For example, the flexibility of prM appeared much higher for ZIKV compared to DENV-2 prM, while regions surrounding N-glycosylation sites of DENV-2 NS1 displayed greater apparent flexibility compared to the corresponding regions of ZIKV NS1. Further studies are required to define the commonalities and differences in sites of genetic flexibility between different flaviviruses and DENV serotypes and the impact of different host cell types and species on this flexibility. In a further refinement of the transposon mutagenesis approach, several recent studies have combined random point mutagenesis with NGS-based analysis of viral fitness to provide comprehensive profiles of the impact of all possible amino acid substitutions in a viral protein with respect to analysis of corresponding high-resolution protein structures (reviewed in (15)). This approach could similarly be applied to great effect for DENV and 574 related flaviviruses. In summary, we propose that variations of the high throughput 575 mutagenesis-coupled genetic profiling approach applied here, in conjunction with increased 576 availability of high-resolution viral protein structural information, may rapidly increase our 577 understanding of the DENV replication cycle and expedite the development of urgently 578 required antiviral therapies and vaccines. 579

replicative fitness, Fulton et al very recently reported the impact of high throughput

580

581 MATERIALS AND METHODS

582 Cell culture

Huh-7.5 cells (40) were generously provided by Charles M. Rice (Rockefeller University,
New York, USA) and were maintained as described previously (41). C6/36 cells, derived

from Aedes albopictus mosquitoes, were generously provided by Jillian M. Carr (Flinders 585 University, Adelaide, Australia) and were cultured at 28°C in a 5% CO₂ atmosphere in Basal 586 Medium Eagle supplemented with MEM non-essential amino acids, sodium pyruvate, 587 GlutaMAX, Penicillin Streptomycin and 10% FBS. Vero cells were generously provided by 588 Jillian M. Carr (Flinders University, Adelaide, Australia) and were cultured as described 589 590 previously (42). All cell culture media and additives were purchased from Thermo Fisher 591 Scientific.

592

593 Antibodies and chemicals

Mouse anti-NS1 mAb 4G4 and mouse anti-dsRNA mAb 3G1 (IgM) were generously 594 provided by Roy Hall (University of Queensland, Brisbane, Australia) (43, 44). Mouse anti-595 capsid mAb 6F3.1 was kindly provided by John Aaskov (Queensland University of 596 Technology, Brisbane, Australia) (45). Mouse anti-B-actin mAb (AC-74) was purchased from 597 Sigma-Aldrich. Rabbit anti-FLAG mAb (D6W5B) was purchased from Cell Signalling 598 Technologies. AlexaFluor 488-, 555- and 647-conjugated secondary antibodies and HRP-599 600 conjugated secondary antibodies were purchased from Thermo Fisher Scientific. 601 Nanchangmycin was purchased from Selleck Chemicals and dissolved in DMSO to 10 mM, 602 aliquoted and stored at -80°C.

603

604 Viruses and plasmids

Plasmid pFK-DVs containing a full-length DENV-2 genome (strain 16681) was generously 605 provide by Ralf Bartenschlager (University of Heidelberg, Heidelberg, Germany) (46). Exact 606 607 details about reporter- and epitope-tagged virus generation are available upon request. To 608 initiate viral RNA replication, DENV plasmids were linearized with XbaI before use as 609 templates in *in vitro* transcription reactions using an mMessage mMachine SP6 Transcription Accepted Manuscript Posted Online

lournal of Virology

kit (Thermo Fisher Scientific) and transfection of viral RNA into Huh-7.5 cells by 610 611 electroporation or transfection with DMRIE-C Reagent (Thermo Fisher Scientific), as described previously (41). Virus infectivity was measured by focus-forming assay. Briefly, 612 Huh-7.5 cells were seeded at 2×10^4 cells/well into 96-well plates and returned to culture 613 overnight prior to inoculation with 40 µl/well of 10-fold serial dilutions of virus-containing 614 cell culture supernatants. Following infection for 3 h at 37°C/5%CO₂, cells were washed once 615 616 with PBS and returned to culture in fresh media for 72 h prior to fixation and 617 immunofluorescent labelling with anti-capsid antibody. Clusters (foci) of infected cells were then enumerated and virus infectivity expressed as focus-forming units per millilitre 618 (FFU/ml). 619

620

Generation of the DENV insertional mutant library 621

Plasmid pFK-DVs was mutagenized using the Mutation Generation System (Thermo Fisher 622 623 Scientific), as per manufacturer's recommendations. Three independent in vitro transposon 624 insertion reactions were performed using 500 ng of plasmid per reaction, pooled and 625 transformed into XL-10 Gold Ultracompetent Cells (Agilent Technologies). Transformants 626 were plated onto 15-cm plates with LB agar containing ampicillin and kanamycin and grown for 18 h at 37°C. Bacterial colonies (~ 2.5×10^5) were then scraped and pooled before 627 extraction of plasmid DNA using a NucleoBond Xtra Midi kit (Macherey-Nagel). Plasmid 628 629 DNA was then digested with NotI-HF (New England Biolabs) to remove the transposon body, gel extracted and re-ligated using T4 DNA ligase (Promega). Approximately 150 ng of 630 ligated plasmid was then transformed into XL-10 Gold cells, as above, and cells were plated 631 632 onto LB agar plates containing ampicillin and cultured grown for 18 h at 37°C. Plasmid DNA was extracted from pooled colonies (~ 2.5×10^5 colonies), as above, and verified by 633 diagnostic restriction digest (not shown). 634

 \geq

635

Mutant Virus Library Passage and Analysis of Transposon Insertion Frequency by RT PCR and Illumina Sequencing

Huh-7.5 cells were electroporated with in vitro-transcribed transposon mutant DENV library 638 RNA. For this, thirteen electroporations were performed with 4×10^6 cells and 10 µg of RNA 639 per electroporation using 0.4 cm cuvettes and a Gene Pulser Xcell Electroporation System 640 (Bio-Rad) to deliver a single pulse (270 V, 100 ohms, 970 µF). Cells were then resuspended 641 in complete media, pooled and plated into thirteen 75 $\rm cm^2$ flasks and returned to culture. 642 Virus replication and spread was monitored in parallel cultures by immunofluorescence and 643 at 6 days post-electroporation, when \sim 50% of cells were infected, cell culture supernatants 644 were collected, cleared by centrifugation and diluted in an equal volume of fresh media 645 before applying to naïve target cells, seeded the previous day into thirteen 75 cm² flasks at 646 1.6×10^6 cells per flask. Total RNA was isolated from electroporated cell monolayers (6 d 647 post-electroporation) and infected cell monolayers (2 d post-infection) using TRIzol (Thermo 648 Fisher Scientific) as per manufacturer's instructions. This cellular RNA (Pool 1 and Pool 2) 649 650 and the 'input' RNA used for electroporation (Pool 0) were reverse-transcribed into cDNA using Superscript III (Thermo Fisher Scientific) and the oligonucleotide DV2NGS6R (see 651 below) as per manufacturer's instructions. Alternatively, the infectious virus-containing 652 653 supernatant from mutant library-electroporated Huh-7.5 cells (see above) was diluted (1:3) in appropriate media and applied to naïve Huh-7.5, Vero or C6/36 cells that had been seeded the 654 previous day into 75 cm² flasks (three flasks per cell type with 1.2×10^6 cells/flask). As 655 656 above, at 2 days post-infection total RNA was extracted from these cells and used to prepare cDNA. In both instances, this cDNA then served as template for PCR to amplify the entire 657 genome in six overlapping fragments using Q5 High-Fidelity DNA polymerase (New 658 659 England Biolabs) and the six following oligonucleotide pairs: DV2NGS1F 5'-

Downloaded from http://jvi.asm.org/ on September 29, 2017 by UNIVERSITY OF EXETER

660	AGTTGTTAGTCTACGTGGACCG-3'	and	DV2NGS1R	5'-
661	CGAATGGAGGTTCTGCTTCTATGT-3';		DV2NGS2F	5'-
662	GCAGAAACACAACATGGAACAATAG-3'	and	DV2NGS2R	5'-
663	CCTAAGGCTAACGCATCAGTC-3';	Ι	DV2NGS3F	5'-
664	TGTCCTTTAGAGACCTGGGAAG-3'	and	DV2NGS3R	5'-
665	ATGTCAGTTGTAACCACGAAGTCC-3';		DV2NGS4F	5'-
666	CAGCAAGTATAGCAGCTAGAGGA-3'	and	NGS4R	5'-
667	TTTCCCTTCTGGTGTGACCATG-3'; DV2NGS5F			5'-
668	CTCAAGTATTGATGATGAGGACTACATG-3	3' a	nd DV2NGS5R	5'-
669	ACTTGTGTCCAATCATTCCATCC-3';		DV2NGS6F	5'-
670	CCGCAGGATGGGATACAAGA-3'	and	DV2NGS6R	5'-
671	AGAACCTGTTGATTCAACAGCAC-3'. PCR	products w	vere then gel-extracted, qu	antified

using a Qubit dsDNA HS Assay Kit (Thermo Fisher Scientific) and combined in equimolar 672 amounts for each pool. Samples were then processed using a Nextera XT Library Preparation 673 674 Kit (Illumina) and sequenced using a NextSeq500 (Illumina) and 150-nt paired-end reads. 675 For analysis, trimmed sequencing reads were filtered for sequences containing the transposon-derived insertion sequence (TGCGGCCGCA), the transposon sequence annotated 676 677 and mapped against the DENV-2 reference sequence (GenBank accession number 678 NC 001474 with minor modifications, as described (46)), using Bowtie 2 (47). The locations of the annotated transposon insertions were then identified from the alignments and counted 679 680 using Geneious version 8 software (48). Original sequencing files are accessible from the 681 NCBI Sequence Reads Archive (SRA) under the series record PRJNA400339.

682

Immunofluorescence Microscopy, Immunoblotting and Luciferase Assays 683

Downloaded from http://jvi.asm.org/ on September 29, 2017 by UNIVERSITY OF EXETER

 688
 Ima,

 689
 soft

 690
 cova

 691
 infer

 692
 fixa

 693
 min

 694
 mAl

 695
 hybr

 696
 twice

 697
 IgG

 698
 (The

 700
 imag

 701
 with

 702
 STE

684

lournal of Virology

lournal of Virology

microscopy for infectivity assays was performed using a Nikon TiE inverted fluorescent 685 microscope system. Confocal fluorescence microscopy was performed using a Zeiss LSM 686 700 confocal microscope system equipped with a $60 \times NA$ 1.4 water-immersion objective. 687 Images were processed using NIS Elements AR v.3.22 (Nikon) and Photoshop 6.0 (Adobe) software. For STED super-resolution imaging, Huh-7.5 cells were cultured overnight on coverslips (18mm round #1.5 glass) that were pre-coated with 0.2% gelatin. Cells were then infected with DENV2-NS1-FLAG (M.O.I.: ~0.1) and returned to culture for 48 h prior to fixation (ice-cold methanol:acetone [1:1], 5 min), washing, blocking (5% BSA in PBS for 30 min at room-temperature) and labelling for 1 h at room temperature with rabbit anti-FLAG mAb (D6W5B; Cell Signalling Technologies diluted 1:200) and anti-dsRNA (mAb 3G1.1 hybridoma supernatant diluted 1:5) diluted in PBS/1% BSA. Samples were then washed twice with PBS before incubation for 1 h at 4°C with Alexa Fluor 488-conjugated anti-rabbit IgG and Alexa Fluor 647-conjugated anti-mouse IgG (cross reactive to IgM) antibodies (Thermo Fisher Scientific) diluted 1:200 in 1%BSA/PBS. Samples were then washed three times and mounted with ProLong Gold (Thermo Fisher Scientific). Samples were then imaged using a Leica TCS SP8 STED 3× microscope system (Leica Microsystems) equipped with 592, 660 and 775 nm STED lasers, using a 100x, NA 1.4 oil objective at 4× zoom. For STED, Alexa Fluor 488 labels were excited with a 488 nm wavelength of a pulsed white light 703 (WL) laser (80 MHz) and depleted with a CW 592 STED laser with a maximum power of 704 1500 mW (typically operating at ~30%). Similarly, for STED Alexa Fluor 647 labels were 705 excited with a 647 nm wavelength of a WL laser and depleted with a CW 775 nm STED laser with a maximum power of 1500 mW (typically operating at \sim 50%). Images were acquired in 706 707 2D STED mode with settings optimized for maximum gains in lateral resolution. Time gates 708 were 0.5-6 ns. A total of 4 z-sections were acquired (0.142 µm z-steps) for both confocal and

Immunofluorescent labelling was performed as described (41). Widefield fluorescence

STED channels and a line averaging of 7 was applied. Deconvolution of confocal and STED 709 710 data (see Fig. 9) was performed using Huygens Professional Deconvolution software (version 14.10; Scientific Volume Imaging) and default settings. Immunoblotting was performed as 711 described (49). Where indicated pre-cleared supernatants were treated with PNGase F (New 712 713 England Biolabs) for 4 hour at 37°C under non-reducing conditions, as per manufacturer's instructions. Western blots were imaged using a ChemiDoc MP Imaging System (Bio-Rad) 714 and, where applicable, band intensities were quantified using Image Lab software (vers. 715 5.2.1; Bio-Rad). Assays of NanoLuc (NLuc) activity were performed as described (50). In 716 brief, Huh-7.5 cells were seeded into 96-well plates at 2×10^4 cells per well and cultured 717 overnight prior to infection with DENV2-NS1-NLuc at the indicated M.O.I., with or without 718 pre-treatment with Nanchangmycin for 1 hour at the indicated concentration (or vehicle 719 control; DMSO at 0.1%). Four hours later cells were then washed and returned to culture for 720 48 h prior to collection of supernatants, washing of monolayers with PBS and lysis using 721 722 Passive Lysis Buffer (Promega). Supernatant samples were cleared by centrifugation and mixed 1:1 with 2 × Passive Lysis Buffer before measurement of NLuc activity in cell lysates 723 724 and supernatants using a Nano-Glo Luciferase Assay System (Promega) and a GloMax 20/20 725 luminometer (Promega).

726

727 Live Cell Imaging

Live cell imaging was performed as described (51). Briefly, DENV2-NS1-mScarlet RNAtransfected Huh-7.5 cells at 4 d post-transfection were seeded onto 0.2% gelatin-coated coverglass bottom dishes (MatTek) and cultured for 2 d in phenol red-free DMEM containing 10% FBS. Alternatively, Huh-7.5 cells were seeded into these dishes at 1.5×10^5 cells per dish, infected the following day at an M.O.I. of ~0.01 and returned to culture for 3 d. Imaging was performed at 37°C using a Nikon TiE inverted fluorescent microscope system equipped

with a heated stage (Okolab), a Plan Apochromat 60× NA 1.4 oil immersion objective 734 735 (Nikon), BrightLine single-band filter sets (DAPI-5060C-NTE-ZERO, FITC-3540C-NTE-736 ZERO and TxRed-4040C-NTE-ZERO; Semrock), a Perfect Focus System (Nikon) and a 737 monochrome 12-bit cooled charge-coupled device camera with a maximum resolution of 738 $1,280 \times 1,024$ (DS-Qi1; Nikon). Illumination was provided by an Intensilight C-HGFIE Precentered Fiber Illuminator mercury light source (Nikon). Images were acquired every 1.5 739 s for 5 mins (Movie S1) or every 10 s for 50 mins (Movie S2). Image processing was 740 performed using NIS Elements v 3.22 software (Nikon), as described in the Figure Legends 741 742 and Supplementary Movie Legends.

743

APEX Electron Microscopy 744

Huh-7.5 cells were seeded into 150 mm cell culture dishes at 1.5×10^6 cells per dish and 745 cultured overnight before mock-infection or infection with DENV2 or DENV2-NS1-APEX2 746 viruses (MOI: ~0.01), prepared as cell culture supernatants collected from electroporated 747 Huh-7.5 cells. At 4 days post-infection, cells were fixed in EM fixative (1.25% 748 glutaraldehyde, 4% paraformaldehyde, 4% sucrose in PBS [pH: 7.2]) for 30 min at 4°C, 749 washed, stained with DAB/H₂O₂ and processed for electron microscopy as described 750 previously (41). Samples were imaged using a Tecnai G2 Spirit transmission electron 751 752 microscope (FEI) operating at 100 kV.

753

Molecular Graphics and Sequence Alignments 754

755 Molecular graphics were performed on the DENV-2 NS1 crystal structure (Protein Data Bank [PDB] accession number 406B) using Pymol version 1.8 molecular visualization system 756 757 (Schrodinger). Sequence alignments of DENV polyprotein sequences were performed using JalView Desktop software with the ClustalW scoring algorithm. The flavivirus isolates with 758

lournal of Virology

the following Uniprot KB/Swiss-Prot accession numbers were compared: DENV-1, *P27909*(Brazil/97-11/1997); DENV-2, *P29991* (Thailand/16681-PDK53); DENV-3, *Q6YMS3*(Martinique/1243/1999); DENV-4 *Q2YHF0* (Thailand/0348/1991); West Nile virus *P06935*;
Yellow Fever virus, *Q6J3P1* (Ivory Coast/1999); Japanese Encephalitis virus *P27395* (SA-14).

764

765 ACKNOWLEDGEMENTS

We are grateful to Ralf Bartenschlager (University of Heidelberg) for the pFK-DVs 766 construct, Charles Rice (The Rockefeller University) for Huh-7.5 cells, Jillian Carr (Flinders 767 University) for Vero cells and C6/36 cells, Roy Hall (University of Queensland) for anti-NS1 768 and anti-dsRNA mAbs and John Aaskov (Queensland University of Technology) for anti-769 capsid mAb. We also thank Kate Pilkington (The Detmold Family Trust Cell Imaging Centre, 770 SA Pathology) for assistance with confocal microscopy, Lyn Waterhouse and Ruth Williams 771 (Adelaide Microscopy, University of Adelaide) for assistance with electron microscopy and 772 Stephen Thompson (Leica Microsystems) for assistance with STED image acquisition and 773 774 processing. DNA sequencing was performed at the Ramaciotti Centre for Genomics (University of New South Wales). This work was funded by grants from the National Health 775 and Medical Research Council (NHMRC) (1027641 and 1053206 to M.R.B.). A.A.E. and 776 R.A.B. are supported by fellowships from the NHMRC (grants 1130128 and 1084706, 777 respectively). The funders had no role in the study design, data collection and interpretation, 778 or the decision to submit the work for publication. 779

780

781 FIGURE LEGENDS

FIG 1. Insertional mutagenesis of the DENV-2 genome and identification of tolerated insertions. (A) Schematic overview of the transposon mutagenesis-coupled next-generation

sequencing (NGS) approach to identify sites within the DENV-2 genome that tolerate small 784 785 (15-nt) insertions. Briefly, Huh-7.5 cells were transfected by electroporation with in vitrotranscribed RNA for the DENV-2 insertional mutant pool (Pool 0). At 6 days post-786 transfection (Pool 1) virus-containing cell culture supernatants were collected and applied to 787 788 naïve target cells for an additional 2 days (Pool 2). Total RNA was extracted from transfected and infected cell monolayers (Pools 1 and 2, respectively) and, together with the input mutant 789 RNA library (Pool 0), was used for RT-PCR and NGS-based quantitation of each insertion 790 mutant. Bar graphs displaying the number of reads containing transposon insertions at each 791 792 nucleotide position are depicted for: (B) the input mutant library (Pool 0); (C) replication-793 competent viruses (Pool 1) and; (D) infectious viruses. (E) Graphical overlay of insert counts 794 for each pool. The colors assigned to each pool are depicted in the legend shown in the lower 795 panel of (A).

796

FIG 2. Tolerance of transposon insertions in DENV-2 expressed as a percentage of the initial 797 input mutant RNA pool. (A) Graph depicting the frequency of insertions in the replication-798 799 competent pool (Pool 1; P1), expressed as a percentage of the frequency of the corresponding mutants in the initial mutant RNA pool (Pool 0; P0). (B) Similarly, the frequency of 800 insertions in the infectious pool (Pool 2; P2) was expressed as a percentage of the frequency 801 802 of the corresponding mutants in the initial mutant RNA pool (Pool 0; PO). Nucleotide positions along the x-axis indicate the junctions of the coding sequences of the individual 803 804 DENV-2 proteins. For clarity the regions encoding the respective DENV-2 proteins are 805 indicated as colored backgrounds. Note that 1 insertion count was added to the raw counts for Pool 0 to enable representation of insertions that only appeared in Pools 1 and/or 2, but not in 806 807 Pool 0. See also Dataset S1.

808

Downloaded from http://jvi.asm.org/ on September 29, 2017 by UNIVERSITY OF EXETER

FIG 3. The DENV-2 NS1 protein is highly tolerant of insertions. (A) The insertional 809 mutagenesis profile within the NS1-encoding region of the DENV-2 genome was examined 810 with respect to NS1 protein domains. In the NS1 schematic the β -roll, Wing and β -ladder 811 812 domains are colored blue, yellow and red, respectively, while *connector* sub-domains are 813 depicted in orange and the location of N-glycosylation sites (N-glyc) are indicated in green. The graph shows an overlay of the number of raw reads for each transposon insertion site in 814 815 Pool 0 (cyan), Pool 1 (magenta) and Pool 2 (yellow) and where they overlap, according to the 816 legend to the right of the graph. The x-axis shows the DENV-2 nucleotide positions of the 817 NS1-encoding region (nucleotides 2422-3477). (B) The location of the 10 most tolerated transposon insertion sites in the NS1 protein, provided that at least two nucleotides within the 818 819 given codon preceded tolerated insertions, are shown as green van der Waals spheres in a 820 ribbon representation of the DENV NS1 dimer structure (Protein Data Bank [PDB] accession 821 no. 406B) (also see Dataset S1). One monomer is shown in gray and the other monomer is 822 colored according to domains as in (A). Insertions at Lys-174, Thr-126 and Ser-204 were 823 highly tolerated. As shown in the perpendicular view (right panel), the most tolerated 824 mutations are relatively distant from the inner hydrophobic face that is pointed downward.

825

FIG 4. Tolerance of transposon insertions within the capsid-encoding sequence. (A) The 826 insertional mutagenesis profile within the capsid-encoding region of the DENV-2 genome 827 828 was examined with respect to capsid protein domains. In the capsid schematic the $\alpha 1$, $\alpha 2$, $\alpha 3$ and $\alpha 4$ alpha helices are colored blue, green, yellow and red, respectively, while the 829 transmembrane anchor is colored gray. The graph in the upper panel shows the distribution of 830 831 insertions in the input mutant RNA pool (Pool 0). The graph in the middle panel shows the number of raw sequencing reads for each insertion in the replication competent pool (Pool 1), 832 while the graph in the lower panel shows the number of reads for each insertion in the 833

infectious virus pool (Pool 2). (B) Graphical overlay of the number of raw reads for each
transposon insertion site in Pool 0 (cyan), Pool 1 (magenta) and Pool 2 (yellow) and where
they overlap, according to the legend below the graph. The *x*-axis shows the DENV-2
nucleotide positions of the capsid-encoding region (nucleotides 97-342).

838

FIG 5. The influence of host cell type on the tolerance of DENV-2 to transposon 839 mutagenesis. (A) Infectious virus-containing cell culture supernatants collected from Huh-7.5 840 cells that were electroporated with the DENV-2 mutant library RNA (see Fig 1A) were 841 applied to naïve Huh-7.5, Vero and C6/36 cells in parallel for 48 hours prior to RNA 842 extraction, RT-PCR and Illumina (NextSeq500) sequencing, according to the depicted 843 schematic diagram. The frequencies of transposon-derived insertions in the DENV-2 genome 844 in infected Huh-7.5 cells (B), Vero cells (C) and C6/36 cells (D) were determined by 845 sequencing. (E) Graphical overlay of normalised insert counts for each pool. The colors 846 assigned to each pool are depicted in the legend shown in the lower panel of (A). (F) 847 Representative immunofluorescent micrographs of parallel cultures of mutant DENV-2-848 infected cells at 48 h post-infection. Anti-E staining and DAPI counter-stained nuclei are 849 850 shown in red and blue, respectively. Scale bars are 100 µm.

851

FIG 6. Characterization of epitope- and reporter-tagged DENV-2 constructs. (A) Guided by the insertional map, a panel of tagged viruses were generated that featured the indicated epitope or reporter protein insertions in capsid, adjacent to the membrane anchor ('CAPmem'), or NS1, immediately downstream of Lys-174. (B) Huh7.5 cells were electroporated with *in vitro* transcribed RNA for the indicated DENV-2 constructs and cultured for 4 d prior to Western blot analysis of NS1 protein. Detection of β-actin served as a loading control. Similarly supernatants from these cells were cleared by centrifugation and

subjected to SDS-PAGE under non-reducing, non-denaturing conditions and Western blotting 859 with anti-NS1 antibody. Numbers below NS1 Western blots indicate levels of NS1 protein in 860 whole cell lysates (normalized to β -actin and expressed as a percentage of wildtype levels 861 862 [%-WT]; upper panel) and extracellular NS1 protein (expressed as a ratio to intracellular NS1 863 bands, with the wildtype ratio set to 1 [Ext:Int]; lower panel). (C) Automated 864 immunofluorescence analysis of the proportion of capsid protein-positive Huh-7.5 cells at 4 d 865 post-electroporation with the indicated DENV-2 RNA transcripts. Data are means + S.D (n = 866 3, for >1500 cells/electroporation). (D) Infectivity titres were determined by focus forming 867 unit (FFU) assays at 24-120 h post-electroporation of Huh-7.5 cells with the indicated DENV-2 RNA transcripts. Data are means + S.D. (n = 3). The dashed line indicates the limit 868 869 of detection of the assay.

870

871 FIG 7. The impact of epitope- and reporter-insertions on NS1 secretion and glycosylation in 872 Huh-7.5 cells and infectious virus production in C6/36 and Vero cell lines. (A) Supernatants 873 were collected at 96 h post-transfection from Huh-7.5 cells transfected with the indicated 874 DENV2 RNA transcripts and cleared of cells and debris by low-speed centrifugation (5,000 875 $\times g$, 5 mins). Samples were subjected to SDS-PAGE under reducing and denaturing conditions (β ME/heat, +) or non-reducing, non-denaturing conditions (β ME/heat, -), as 876 877 indicated, and Western blotting was performed using anti-NS1 mAb 4G4. Secreted NS1 was strongly detected under non-denaturing, non-reducing conditions for wildtype and tagged 878 879 viruses alike. (B) Supernatant samples were also subjected to de-glycosylation using PNGase 880 F under non-denaturing conditions (4 h at 37°C) or mock-treated, before SDS-PAGE under non-reducing, non-denaturing conditions and Western blotting with anti-NS1 mAb 4G4. A 881 similar shift in electrophoretic mobility was observed for wildtype and tagged NS1 proteins 882 883 following PNGase F treatment. (C-D) Infectious virus production by C6/36 cells and Vero

cells transfected with epitope- and reporter-tagged DENV2 RNA transcripts. (C) C6/36 cells 884 and (D) Vero cells were transfected with the indicated DENV2 RNA transcripts and returned 885 to culture before collection of supernatant samples at the indicated time-points (24-120 h). 886 Infectivity of supernatants were determined by focus-forming assay. Data are means + S.D. 887 (n = 3). The dashed line indicates the limit of detection. 888

889

FIG 8. Localization of NS1 with respect to dsRNA and capsid is unaltered for epitope- and 890 reporter-tagged DENV-2 viruses. Huh-7.5 cells were transfected with in vitro-transcribed 891 RNA for DENV2 and NS1- and capsid-tagged DENV2 derivatives and cultured for 96 h prior 892 893 to fixation and sequential indirect immunofluorescent labelling using anti-dsRNA (mAb 3G1) 894 and Alexa Fluor 555-conjugated anti-mouse IgM (red), followed by either: (A) anti-NS1 (mAb 4G4) and Alexa Fluor 488-conjugated anti-mouse IgG (green) or; (B) anti-capsid 895 (mAb 6F3.1) and Alexa Fluor 488-conjugated anti-mouse IgG (green). Samples were 896 counterstained with DAPI (blue) and analysed by confocal fluorescence microscopy. Yellow 897 in the merged images indicates co-localization. Pearson's co-localization coefficients are 898 indicated in white in the merged images (means \pm S.D. for n = 3-5 [stitched] fields of 203 \times 899 203 μ m, each containing >10 cells). 'Insets' represent zoomed images of the boxed areas in 900 901 the 'Merge' panels. Scale bars are 10 µm.

902

903 FIG 9. Sensitive monitoring of intracellular and secreted levels of NanoLuc-tagged NS1 904 following infection with DENV2-NS1-NLuc. (A) Huh-7.5 cells in 96-well plates were infected with DENV2-NS1-NLuc at the indicated multiplicity of infection (M.O.I.) for 4 h, 905 906 washed and returned to culture for 48 h prior to determination of intracellular and 907 extracellular NanoLuc activity. (B) Semi-confluent Huh-7.5 cells in 96-well trays were 908 treated with the indicated concentration of Nanchangmycin for 1 hour, prior to infection with

lournal of Virology

909 DENV2-NS1-NLuc (M.O.I.: ~0.05) for 4 h. Cells were then washed and returned to culture 910 for 48 h prior to measurement of intracellular and extracellular NLuc activity. Data are means 911 \pm S.D. (n = 4). Results are representative of similar repeat experiments.

912

913 FIG 10. APEX electron microscopy analysis of NS1 localization. Huh-7.5 cells were mock-914 infected or infected with untagged DENV2 or DENV2-NS1-APEX2 (M.O.I. ~0.01) and cultured for 96 h prior to fixation and labelling with DAB/H₂O₂. (A) Light microscopy 915 revealed the presence of DAB polymerization only in DENV2-NS1-APEX2-infected cells 916 (right panel). Scale bars are 100 µm. (B) Samples were then processed for EM. Compared to 917 918 mock-infected cells (not shown), DENV2-infected cells (upper panels) displayed 919 characteristic virus-induced ER rearrangements including CMs (see 'ii') and VPs (see 'ii'). 920 Scale bars are 500, 200, 500 and 100 nm, left-to-right, as indicated. In contrast, DENV2-921 NS1-APEX2-infected cells revealed discernible DAB deposition in the Golgi apparatus 922 ('iii'), ER membranes (see 'ER' arrowheads in 'iv') and intense diffuse staining of VP 923 membranes and punctate staining of the VP interior (see 'zoom inset'). Scale bars are 1000, 924 100, 500 and 100 nm, left-to-right, as indicated. Enlarged views are shown to the right of 925 each boxed area. In addition to localization to the surface and interior of VPs (see yellow arrows in 'v'), NS1-APEX2 was also detected in irregular punctae that were adjacent to VPs 926 (see yellow arrowheads in 'v'). Furthermore, NS1-APEX2 was less frequently identified in 927 928 regular arrays (see cyan arrowheads in 'vi') that featured more diffuse membrane staining and punctate luminal staining. Scale bars for 'v' and 'vi' are 100 nm and 200 nm, 929 respectively. CM, convoluted membranes; mit, mitochondrium; VP, vesicle packet; ER, 930 931 endoplasmic reticulum; LD, lipid droplet.

932

FIG 11. STED super-resolution imaging of NS1 and dsRNA localization in infected cells. 933 934 Huh-7.5 cells were infected with DENV2-NS1-FLAG (M.O.I.: ~0.1) and returned to culture 935 for 48 h prior to fixation and indirect immunofluorescent labelling using anti-FLAG (Alexa Fluor-488, green) and anti-dsRNA (Alexa Fluor-647; red) as described in Materials and 936 937 Methods. Samples were then mounted and imaged using a Leica TCS SP8 STED 3× 938 microscope system (Leica Microsystems) equipped with 592, 660 and 775 nm STED lasers using a 100x, NA 1.4 oil objective at $4 \times$ zoom. Confocal and STED images (in 2D STED 939 mode) were acquired sequentially, as described in Materials and Methods. Imaging data for 940 both confocal imaging and STED imaging were deconvolved using Huygens Professional 941 Deconvolution software (version 14.10; Scientific Volume Imaging) applying default 942 settings. A single optical section for confocal (A) and STED (B) channels is depicted. Scale 943 bars are 5 µm for main images and 500 nm for 'insets'. 944

945

FIG 12. Live cell imaging of mScarlet-tagged NS1 in infected cells. (A) Schematic diagram 946 of the DENV2-NS1-mScarlet construct. (B-C) Infectivity of DENV2-NS1-mScarlet 947 compared to wildtype DENV-2. Huh-7.5 cells were transfected with wildtype DENV-2 or 948 DENV2-NS1-mScarlet RNA transcripts and cell culture supernatants were collected at 24-949 120 h post-transfection for determination of virus infectivity by focus-forming assay (FFA). 950 (B) The immunofluorescent micrographs show representative images from a FFA of cells 951 infected with undiluted DENV-2 or DENV2-NS1-mScarlet supernatants collected at 120 h 952 post-transfection. Cells were labelled with anti-E antibody (green) and mScarlet-associated 953 epifluorescence was also visualised (red). Scale bars are 100 µm. (C) Quantitation of 954 955 infectivity by FFA. Data are means + S.D. (n = 3). The dashed line indicates the limit of detection. n.d., not detectable. (D-E) Live cell imaging of Huh-7.5 cells transfected with 956 DENV2-NS1-mScarlet transcripts (6 d post-transfection). (D) Detection of mScarlet 957

autofluorescence in live Huh-7.5 cells following mock-transfection ('Mock') or transfection 958 DENV2-NS1-mScarlet RNA transcripts. Scale bars are 100 µm. (E) Live cell imaging of 959 NS1-mScarlet localization and traffic. Insets depict examples of intensely fluorescent, 960 relatively static NS1-mScarlet foci (cyan arrows) and weakly fluorescent, highly motile NS1-961 mScarlet foci (cyan arrowheads). See also Supplementary Movie 1. Scale bars are 10 µm for 962 963 the main image and 5 μ m for insets.

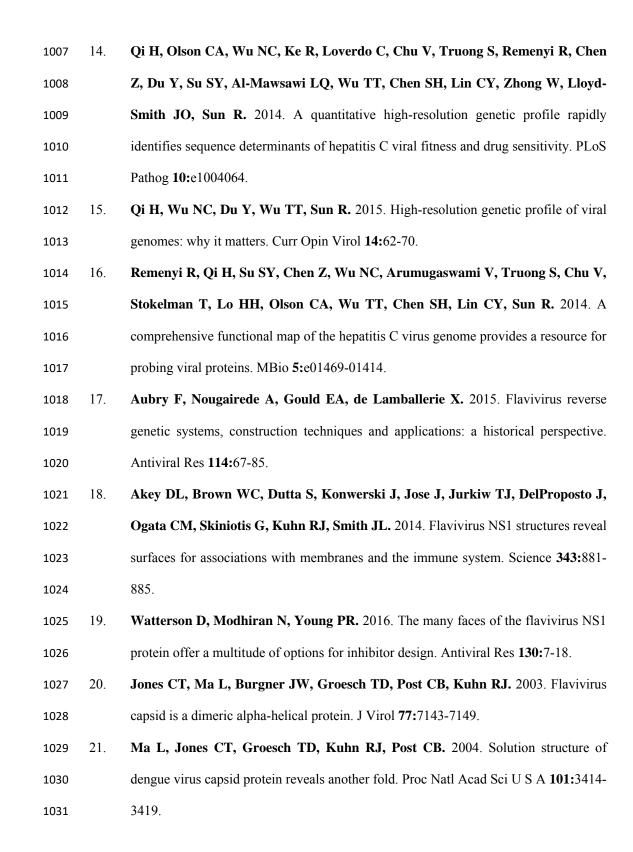
964

REFERENCES 965

- Bhatt S, Gething PW, Brady OJ, Messina JP, Farlow AW, Moyes CL, Drake 966 1. JM, Brownstein JS, Hoen AG, Sankoh O, Myers MF, George DB, Jaenisch T, 967 Wint GR, Simmons CP, Scott TW, Farrar JJ, Hay SI. 2013. The global 968 distribution and burden of dengue. Nature 496:504-507. 969
- 2. Deen J. 2016. The Dengue Vaccine Dilemma: Balancing the Individual and 970 Population Risks and Benefits. PLoS Med 13:e1002182. 971
- 3. Chatel-Chaix L, Bartenschlager R. 2014. Dengue virus- and hepatitis C virus-972 induced replication and assembly compartments: the enemy inside--caught in the web. 973 J Virol 88:5907-5911. 974
- Welsch S, Miller S, Romero-Brey I, Merz A, Bleck CK, Walther P, Fuller SD, 975 4. Antony C, Krijnse-Locker J, Bartenschlager R. 2009. Composition and three-976 dimensional architecture of the dengue virus replication and assembly sites. Cell Host 977 Microbe 5:365-375. 978
- Westaway EG, Mackenzie JM, Kenney MT, Jones MK, Khromykh AA. 1997. 979 5. Ultrastructure of Kunjin virus-infected cells: colocalization of NS1 and NS3 with 980 981 double-stranded RNA, and of NS2B with NS3, in virus-induced membrane structures. J Virol **71:**6650-6661. 982

986 7. Gebhard LG, Iglesias NG, Byk LA, Filomatori CV, De Maio FA, Gamarnik AV.
987 2016. A Proline-Rich N-Terminal Region of the Dengue Virus NS3 Is Crucial for
988 Infectious Particle Production. J Virol 90:5451-5461.

- Scaturro P, Cortese M, Chatel-Chaix L, Fischl W, Bartenschlager R. 2015.
 Dengue Virus Non-structural Protein 1 Modulates Infectious Particle Production via
 Interaction with the Structural Proteins. PLoS Pathog 11:e1005277.
- Wu RH, Tsai MH, Chao DY, Yueh A. 2015. Scanning mutagenesis studies reveal a
 potential intramolecular interaction within the C-terminal half of dengue virus NS2A
 involved in viral RNA replication and virus assembly and secretion. J Virol 89:4281 4295.
- 10. Xie X, Zou J, Puttikhunt C, Yuan Z, Shi PY. 2015. Two distinct sets of NS2A
 molecules are responsible for dengue virus RNA synthesis and virion assembly. J
 Virol 89:1298-1313.
- 999 11. Roby JA, Setoh YX, Hall RA, Khromykh AA. 2015. Post-translational regulation
 and modifications of flavivirus structural proteins. J Gen Virol 96:1551-1569.
- 1001 12. Fulton BO, Sachs D, Beaty SM, Won ST, Lee B, Palese P, Heaton NS. 2015.
 1002 Mutational Analysis of Measles Virus Suggests Constraints on Antigenic Variation of
 1003 the Glycoproteins. Cell Rep 11:1331-1338.
- 1004 13. Heaton NS, Sachs D, Chen CJ, Hai R, Palese P. 2013. Genome-wide mutagenesis
 1005 of influenza virus reveals unique plasticity of the hemagglutinin and NS1 proteins.
 1006 Proc Natl Acad Sci U S A 110:20248-20253.



42

22. 1032 Byk LA, Gamarnik AV. 2016. Properties and Functions of the Dengue Virus Capsid Protein. Annu Rev Virol 3:263-281. 1033

- 23. Samsa MM, Mondotte JA, Iglesias NG, Assuncao-Miranda I, Barbosa-Lima G, 1034
- Da Poian AT, Bozza PT, Gamarnik AV. 2009. Dengue virus capsid protein usurps 1035 lipid droplets for viral particle formation. PLoS Pathog 5:e1000632. 1036
- Dixon AS, Schwinn MK, Hall MP, Zimmerman K, Otto P, Lubben TH, Butler 24. 1037 BL, Binkowski BF, Machleidt T, Kirkland TA, Wood MG, Eggers CT, Encell 1038 1039 LP, Wood KV. 2016. NanoLuc Complementation Reporter Optimized for Accurate Measurement of Protein Interactions in Cells. ACS Chem Biol 11:400-408. 1040
- 25. Kamiyama D, Sekine S, Barsi-Rhyne B, Hu J, Chen B, Gilbert LA, Ishikawa H, 1041 1042 Leonetti MD, Marshall WF, Weissman JS, Huang B. 2016. Versatile protein 1043 tagging in cells with split fluorescent protein. Nat Commun 7:11046.
- 26. Lam SS, Martell JD, Kamer KJ, Deerinck TJ, Ellisman MH, Mootha VK, Ting 1044 AY. 2015. Directed evolution of APEX2 for electron microscopy and proximity 1045 1046 labeling. Nat Methods 12:51-54.
- 27. Martell JD, Deerinck TJ, Sancak Y, Poulos TL, Mootha VK, Sosinsky GE, 1047 Ellisman MH, Ting AY. 2012. Engineered ascorbate peroxidase as a genetically 1048 encoded reporter for electron microscopy. Nat Biotechnol 30:1143-1148. 1049
- 28. Hall MP, Unch J, Binkowski BF, Valley MP, Butler BL, Wood MG, Otto P, 1050 Zimmerman K, Vidugiris G, Machleidt T, Robers MB, Benink HA, Eggers CT, 1051 Slater MR, Meisenheimer PL, Klaubert DH, Fan F, Encell LP, Wood KV. 2012. 1052
- Engineered luciferase reporter from a deep sea shrimp utilizing a novel 1053 imidazopyrazinone substrate. ACS Chem Biol 7:1848-1857. 1054
- 1055 29. Rausch K, Hackett BA, Weinbren NL, Reeder SM, Sadovsky Y, Hunter CA, Schultz DC, Coyne CB, Cherry S. 2017. Screening Bioactives Reveals 1056

43

- Mackenzie JM, Jones MK, Young PR. 1996. Immunolocalization of the dengue 30. 1059 virus nonstructural glycoprotein NS1 suggests a role in viral RNA replication. 1060 Virology 220:232-240. 1061
- 1062 31. Feng S, Sekine S, Pessino V, Li H, Leonetti MD, Huang B. 2017. Improved split fluorescent proteins for endogenous protein labeling. Nat Commun 8:370. 1063
- 32. Bindels DS, Haarbosch L, van Weeren L, Postma M, Wiese KE, Mastop M, 1064

1065 Aumonier S, Gotthard G, Royant A, Hink MA, Gadella TW, Jr. 2017. mScarlet: a

bright monomeric red fluorescent protein for cellular imaging. Nat Methods 14:53-56. 1066

- Lee CM, Xie X, Zou J, Li SH, Lee MY, Dong H, Qin CF, Kang C, Shi PY. 2015. 1067 33.
- Determinants of Dengue Virus NS4A Protein Oligomerization. J Virol 89:6171-6183. 1068
- 34. Stern O, Hung YF, Valdau O, Yaffe Y, Harris E, Hoffmann S, Willbold D, Sklan 1069 EH. 2013. An N-terminal amphipathic helix in dengue virus nonstructural protein 4A 1070 1071 mediates oligomerization and is essential for replication. J Virol 87:4080-4085.
- 35. Villordo SM, Carballeda JM, Filomatori CV, Gamarnik AV. 2016. RNA 1072
- Structure Duplications and Flavivirus Host Adaptation. Trends Microbiol 24:270-283. 1073
- Villordo SM, Filomatori CV, Sanchez-Vargas I, Blair CD, Gamarnik AV. 2015. 1074 36.

Dengue virus RNA structure specialization facilitates host adaptation. PLoS Pathog 1075 **11:**e1004604. 1076

- 37. Youn S, Li T, McCune BT, Edeling MA, Fremont DH, Cristea IM, Diamond MS. 1077 2012. Evidence for a genetic and physical interaction between nonstructural proteins 1078 NS1 and NS4B that modulates replication of West Nile virus. J Virol 86:7360-7371. 1079
- 1080 38. Richner JM, Jagger BW, Shan C, Fontes CR, Dowd KA, Cao B, Himansu S, Caine EA, Nunes BTD, Medeiros DBA, Muruato AE, Foreman BM, Luo H, 1081

Wang T, Barrett AD, Weaver SC, Vasconcelos PFC, Rossi SL, Ciaramella G, 1082 Mysorekar IU, Pierson TC, Shi PY, Diamond MS. 2017. Vaccine Mediated 1083 Protection Against Zika Virus-Induced Congenital Disease. Cell 170:273-283 e212. 1084

- Fulton BO, Sachs D, Schwarz MC, Palese P, Evans MJ. 2017. Transposon 39. 1085 Mutagenesis of the Zika Virus Genome Highlights Regions Essential for RNA 1086 1087 Replication and Restricted for Immune Evasion. J Virol 91.
- Blight KJ, McKeating JA, Rice CM. 2002. Highly permissive cell lines for 40. 1088 subgenomic and genomic hepatitis C virus RNA replication. J Virol 76:13001-13014. 1089
- Eyre NS, Hampton-Smith RJ, Aloia AL, Eddes JS, Simpson KJ, Hoffmann P, 1090 41. Beard MR. 2016. Phosphorylation of NS5A Serine-235 is essential to hepatitis C 1091 virus RNA replication and normal replication compartment formation. Virology 1092 **491:**27-44. 1093
- Van der Hoek KH, Eyre NS, Shue B, Khantisitthiporn O, Glab-Ampi K, Carr 42. 1094 JM, Gartner MJ, Jolly LA, Thomas PQ, Adikusuma F, Jankovic-Karasoulos T, 1095 Roberts CT, Helbig KJ, Beard MR. 2017. Viperin is an important host restriction 1096 factor in control of Zika virus infection. Sci Rep 7:4475. 1097
- 43. Clark DC, Lobigs M, Lee E, Howard MJ, Clark K, Blitvich BJ, Hall RA. 2007. In 1098 situ reactions of monoclonal antibodies with a viable mutant of Murray Valley 1099 encephalitis virus reveal an absence of dimeric NS1 protein. J Gen Virol 88:1175-1100 1183. 1101
- 44. O'Brien CA, Hobson-Peters J, Yam AW, Colmant AM, McLean BJ, Prow NA, 1102 Watterson D, Hall-Mendelin S, Warrilow D, Ng ML, Khromykh AA, Hall RA. 1103 2015. Viral RNA intermediates as targets for detection and discovery of novel and 1104 1105 emerging mosquito-borne viruses. PLoS Negl Trop Dis 9:e0003629.

<u>Journal</u> of Virology

45.

1106

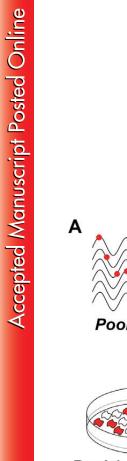
detected with monoclonal antibodies. J Gen Virol 73 (Pt 11):2999-3003. 1107 1108 46. Fischl W, Bartenschlager R. 2013. High-throughput screening using dengue virus reporter genomes. Methods Mol Biol 1030:205-219. 1109 1110 47. Langmead B, Salzberg SL. 2012. Fast gapped-read alignment with Bowtie 2. Nat 1111 Methods 9:357-359. Kearse M, Moir R, Wilson A, Stones-Havas S, Cheung M, Sturrock S, Buxton S, 48. 1112 Cooper A, Markowitz S, Duran C, Thierer T, Ashton B, Meintjes P, Drummond 1113 A. 2012. Geneious Basic: an integrated and extendable desktop software platform for 1114 the organization and analysis of sequence data. Bioinformatics 28:1647-1649. 1115 49. Eyre NS, Drummer HE, Beard MR. 2010. The SR-BI partner PDZK1 facilitates 1116 hepatitis C virus entry. PLoS Pathog 6:e1001130. 1117 50. Eyre NS, Aloia AL, Joyce MA, Chulanetra M, Tyrrell DL, Beard MR. 2017. 1118 Sensitive luminescent reporter viruses reveal appreciable release of hepatitis C virus 1119 NS5A protein into the extracellular environment. Virology 507:20-31. 1120 1121 51. Eyre NS, Fiches GN, Aloia AL, Helbig KJ, McCartney EM, McErlean CS, Li K,

Bulich R, Aaskov JG. 1992. Nuclear localization of dengue 2 virus core protein

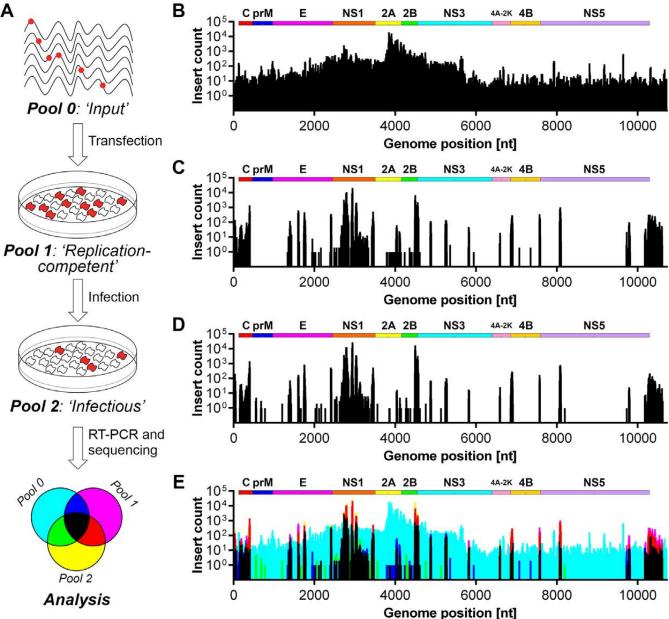
- 1122 Aggarwal A, Turville SG, Beard MR. 2014. Dynamic imaging of the hepatitis C
- 1123 virus NS5A protein during a productive infection. J Virol **88:**3636-3652.

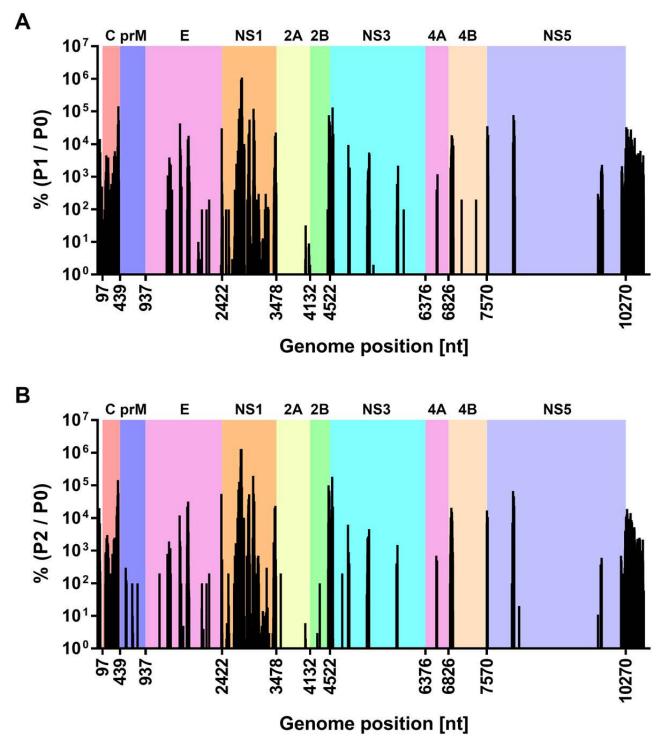
1124

1125

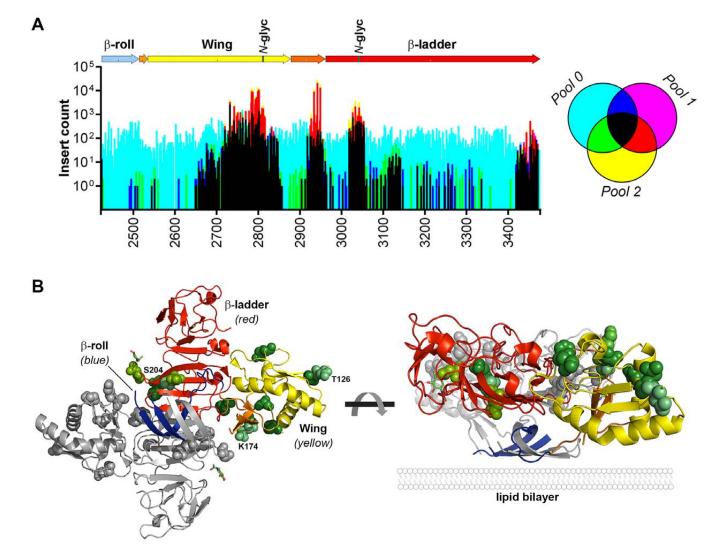




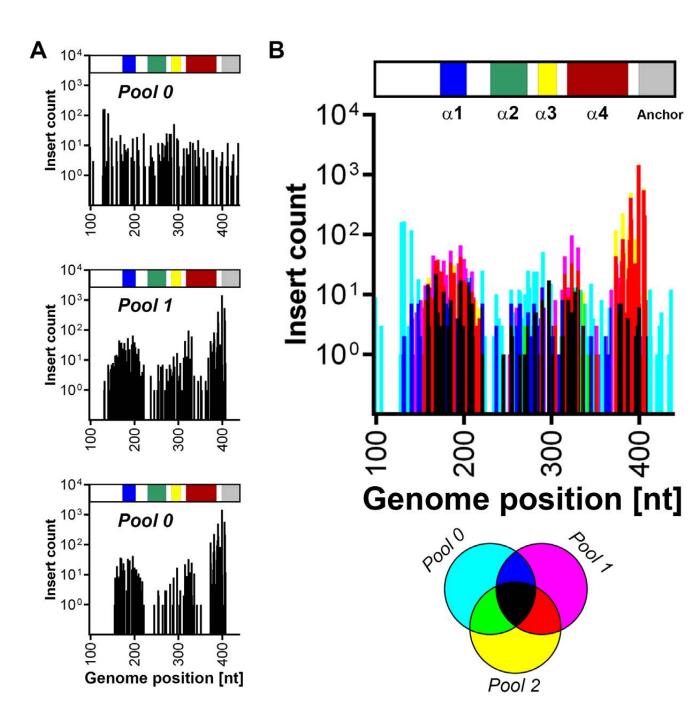




Z



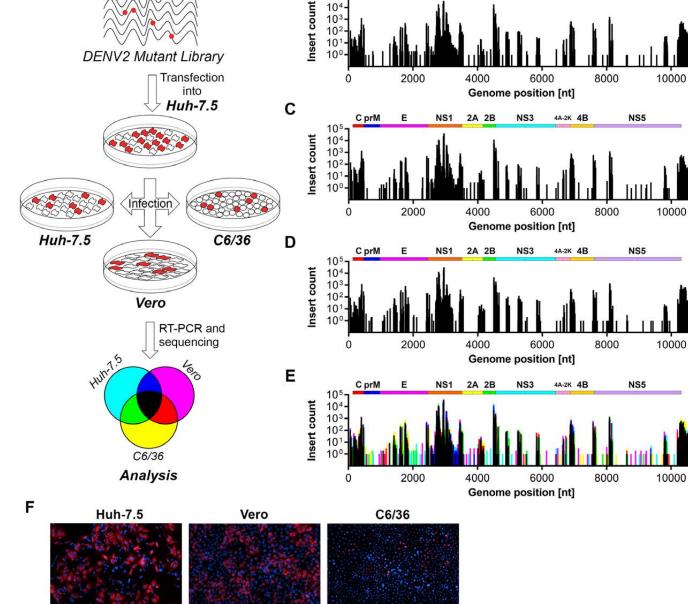
 \leq



Z



Α



в

C prM

105

104

Е

NS1

2A 2B

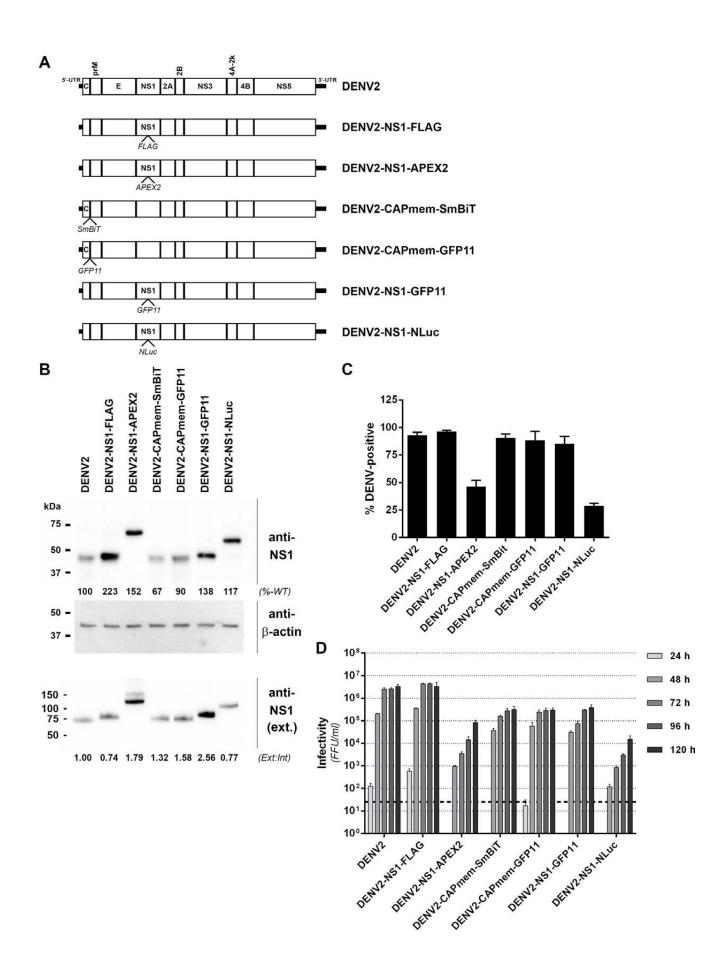
NS3

4A-2K 4B

NS5

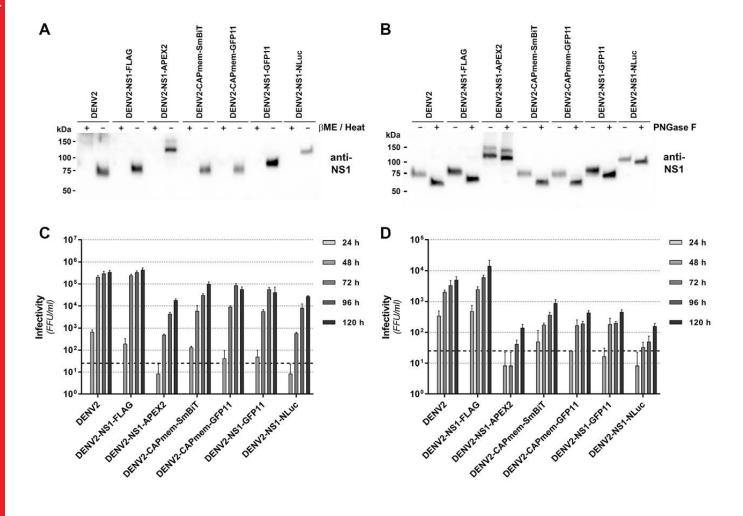


 \sum



Journal of Virology

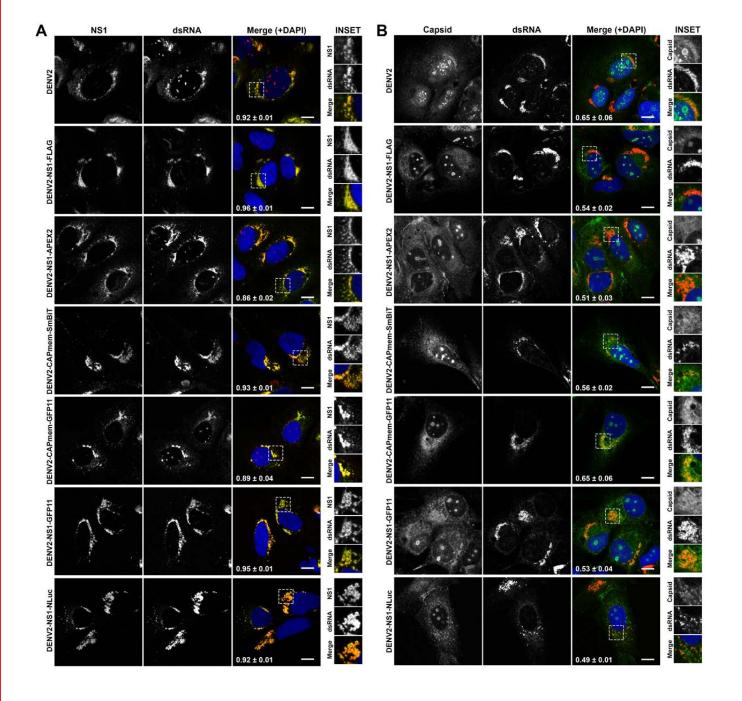
Z

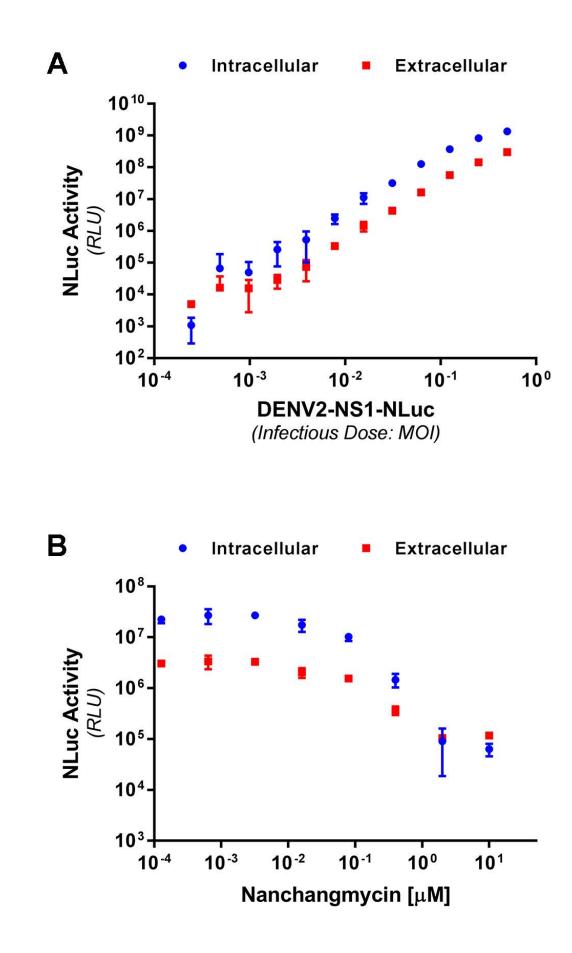


Downloaded from http://jvi.asm.org/ on September 29, 2017 by UNIVERSITY OF EXETER

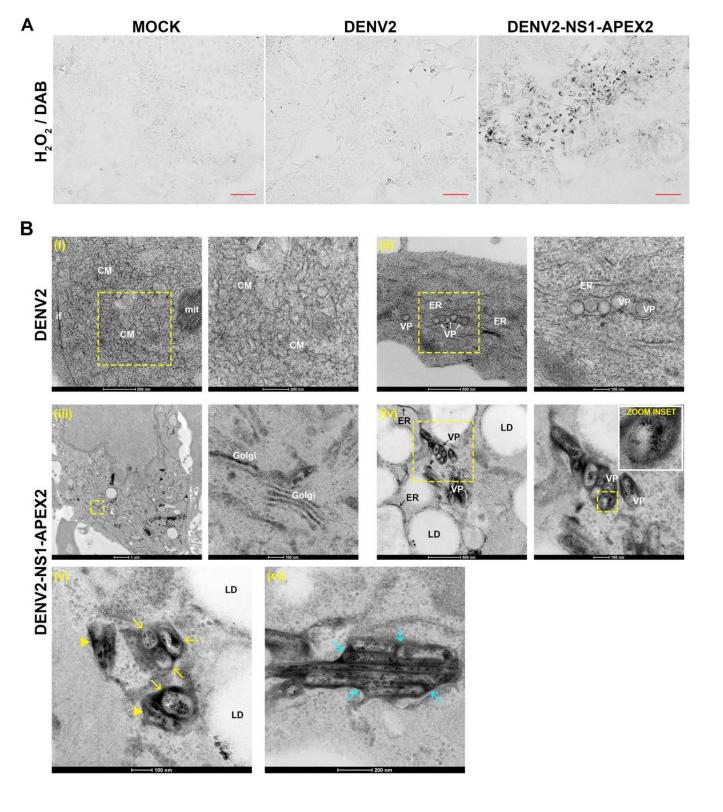


Z



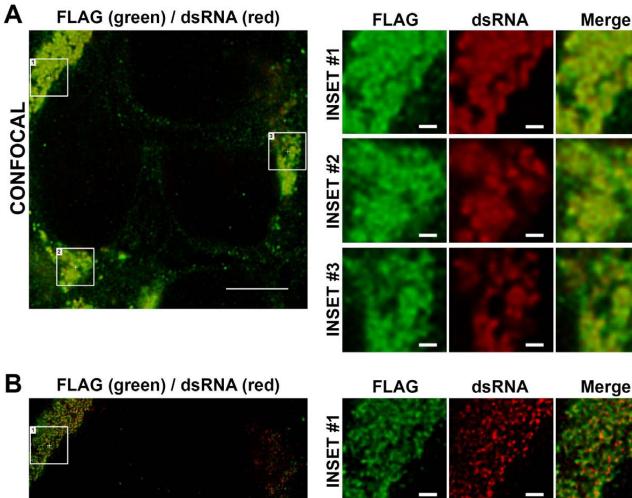


Z



 \leq

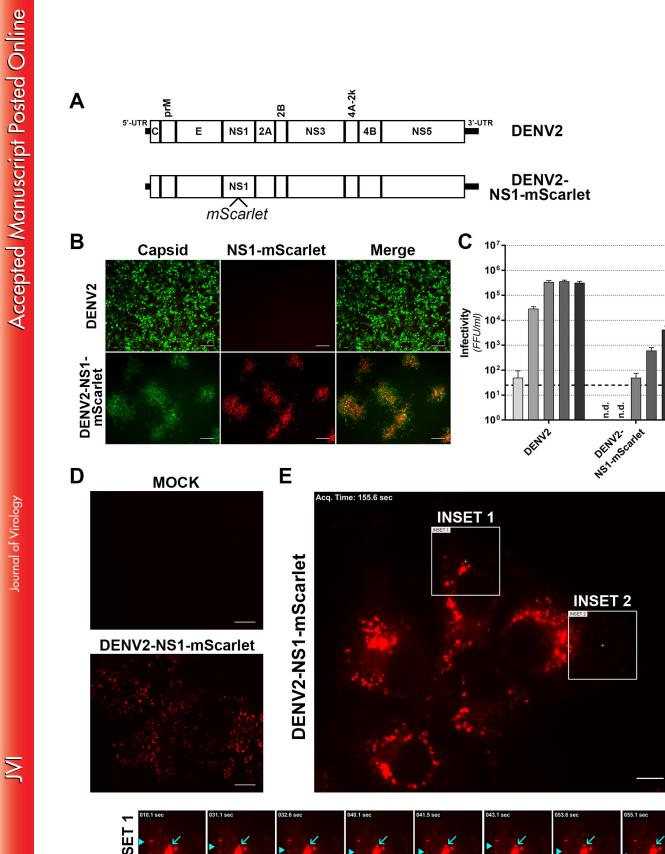
STED



INSET #2

INSET #3

Ŋ



24 h

48 h

72 h

96 h 120 h

